Universitatea "Babeş-Bolyai"
Facultatea de Fizică
Şcoala Doctorală de Fizică

Horia Paşca

Cluster approach to fission

Doctoral thesis summary

Thesis advisor
Prof. dr. Grigore DAMIAN

Cluj-Napoca, 2017

Acknowledgements

I would like to express my immense gratitude to my advisor, Prof. Dr. G. Damian, for his continuous support and motivation. His guidance helped me in all the time of research and writing of this thesis

Besides my advisor, my sincere and enormous gratitude go to Dr. G.G. Adamian and Dr. N.V. Antonenko, who provided me the opportunity to join their team, and who gave me the possibility to work closely with them. Without their patience, motivation, vast knowledge and support it would not be possible to conduct this research.

I would also like to thank Dr. A.V. Andreev for his time and fruitful discussions over the years. His help is immensely appreciated. I would like to thank the rest of my colleagues as well, for the stimulating discussions and questions.

Special thanks go to Prof. Dr. Gh. Adam, Prof. Dr. S. Adam and Prof. Dr. R.V. Jolos for all the advice and help provided over the years.

Last but not the least, I would like to thank my family for always being by my side and constantly encouraging me.

Contents

Introduction

Since the discovery of nuclear fission great attempts have been made in order to understand it from an energetic point of view. In all models, the calculation of the potential energy surfaces (PES) is rather crucial, as all experimental observables are notoriously susceptible to them. Because the PES depends on the collective degrees of freedom, the choice of the relevant collective coordinates is a challenge in itself, as a large number of coordinates rapidly leads to unnecessary complications and parameterizations without any physical meaning, while a small number of coordinates does not depict the entire process, and can hide some of the finer features of the fission process.

The present work aims to provide a simple, clear and concise description of the fission process by employing an improved version of the scission-point model, the DNS model, which is under constant development. The author points out that the present prescription lacks any adjustable or free parameters, and the model starts from experimentally controllable quantities, such as mass, charge and kinetic energies of the target and projectile, and ends up giving measurable results: mass/charge-, TKE- and isotopic-distributions and neutron and gamma multiplicities.

In **the second Chapter** a detailed description of the model is presented, starting from the concept of a di-nuclear system (DNS). The most part of this Chapter is dedicated to the calculation of the total energy of the fissioning system. The starting point is the geometrical description of the system, and the definition of the number of parameters needed for its description. The interaction potential is then tackled, giving a greater attention to it's analysis, analysis that allows us to greatly reduce the number of coordinates. Then, the method of calculation of the binding energies of the nuclei is presented. The Liquid Drop Model (LDM) terms are treated as a function of the nuclei's isotopic components and their deformation. To the macroscopic part, the shell correction terms are added, using the Strutinski method and the two-center shell model. The excitation energy and it's effect on the binding energy is discussed later. At the end of the chapter, the statistical model is described.

The third Chapter is dedicated to the results obtained by deploying the model discussed in the previous Chapter. The theoretical charge, mass and isotopic distributions are presented and compared with the existing experimental data for a large number of fissioning nuclei at fixed energy. The transition from the symmetric fission to the asymmetric one is addressed. The evolution of these distributions with increasing excitation energy makes the subject of the next part of the study. The agreement with the experimental data is very good. For fissioning Th isotopes large asymmetric modes are predicted, as opposed with the existing models. Furthermore, our model predicts the existence of isotonic nuclei ($N \sim 136$), for which the asymmetric fission component bears equal weight to the symmetric one. In the last part of the Chapter the Total Kinetic Energy (TKE) distribution of fission fragments are presented for a series of reactions at different energy. Once again, the comparison with the experimental data shows a good agreement. The author hopes that the presented results presented here will open the doors for new experiments, to prove, or disprove the validity of the results.

The theoretical description of heavy-ion collisions are the subject of the **fourth Chapter**. The main goal is the calculation of the angular momenta of the fission fragments. Here, the author identifies two sources for the intrinsic spin of the fragments: an orbital component, which is responsible for the transfer of the initial angular momentum of the system to the fission fragments, and a collective component, which is the result of the thermal excitation of rotational-vibrational modes of the scission configuration. The last part of this Chapter is dedicated to the fluctuations of the absolute values of the angular momentum around the average value.

In the **fifth Chapter** the theoretical calculations are compared with experimental data. The importance of employing the DNS model is highlighted. Next, the role of the entrance channel is discussed by studying the effect of the bombarding energy and the mass asymmetry on the spin distribution. The author predicts here a saturation of the orbital angular momentum at large bombarding energies. Once again, excellent results are obtained.

The **final Chapter** is dedicated to the final conclusions based on the results in this work.

Theoretical framework

2.1 The concept of a dinuclear system

One of the main challenges in the theoretical study of fission is the description of the transition from a mono-nucleus configuration towards a configuration with two (or more) individualized, separate nuclei (di-nuclear system or DNS). With the advent of the two-center shell model (described in Chapter 2.2.4), the single-particle structure of a scission configuration (with or without the existence of a "neck") could be calculated. It was soon found out ([1], [2]) that the single particle spectra of the scission configuration resembles the single particle levels of the individual nascent fragments directly after scission (the so-called "separability principle"). The author will note here that this is a far-reaching conclusion, as it implies that the primary fragment is almost completely indifferent about the way it is formed. In other words, a ^{112}Pd nucleus has the same properties, regardless if it's formed in the fission of U or Th (it retains, of course, a "memory" of the initial system, such as the total energy and angular momentum, due to conservation laws). This, in turn, allows for a straight-forward description of the scission configuration: two individualized fragments which interact via long-distance Coulomb forces and short-distance nuclear forces - a dinuclear system (DNS).

With the intention of still remaining model-independent at this point and without going into technical details, a few properties of the DNS are worth mentioning:

1. The DNS is formed in the last stages of the fission procces. The two fragments are well individualized, separated by a small distance (there is no overlap between their nuclear densities), but they mutually interact. The individuality of the fragments can be understood on the basis that the the wave functions describing the two nuclei are essentially localized and "walled in" in two distinct potential wells.

2. The DNS is an unstable configuration. Its motion takes place across several coordinates:

(a) *the inter-nuclear distance*: the two nuclei can drift apart, which results in fission;

(b) *the mass and charge coordinates*: the nuclei can exchange the weakly bound nucleons of the upper shells [3]

(c) *the deformation coordinates*: the Coulomb forces, which tend to push the nuclei apart, compete with the short-range nuclear forces, which tend to pull them together; the resulting push-pull interaction tends to elongate both nuclei;

(d) *the rotational coordinates*: in the case of off-center heavy-ion collision there is a certain amount of angular momentum injected to the system, and the entire DNS will rotate around its center of mass due to the angular momentum conservation law. Furthermore, due to the excitation energy accumulated by the system, the angular-momentum-bearing modes are thermally activated, thus the individual fragments can rotate around all three axis, with the condition that the total angular momentum is conserved.

3. The motion of the system in all coordinates is governed by the potential energy of the system.

4. Due to a fast establishing of thermal equilibrium the motion of the system in the mass and charge coordinate is statistical in nature.

2.2 The potential energy

2.2.1 Geometry of the system

The system is modeled as two axially symmetric deformed ellipsoids. The parameters which describe the DNS are the mass and charge numbers A_i, Z_i, deformation parameters β_i and their relative distance d between the surfaces. The index $i = L, H$ designates the light (L) or heavy (H) nuclei.

Before neutron evaporation, the following relations hold: $A_L + A_H = A_{C.N.}$ and $Z_L + Z_H = Z_{C.N.}$. From here on the acronym "C.N." designates the Compound Nucleus, i.e. the initial fissioning system. It is customary that the number of neutrons to be denoted by N and it is linked to the mass and charge number by $N_i = A_i - Z_i$.

The deformations of the two fragments is depicted by the parameter β_i. In the current work, the deformation parameter is defined as the ratio be-

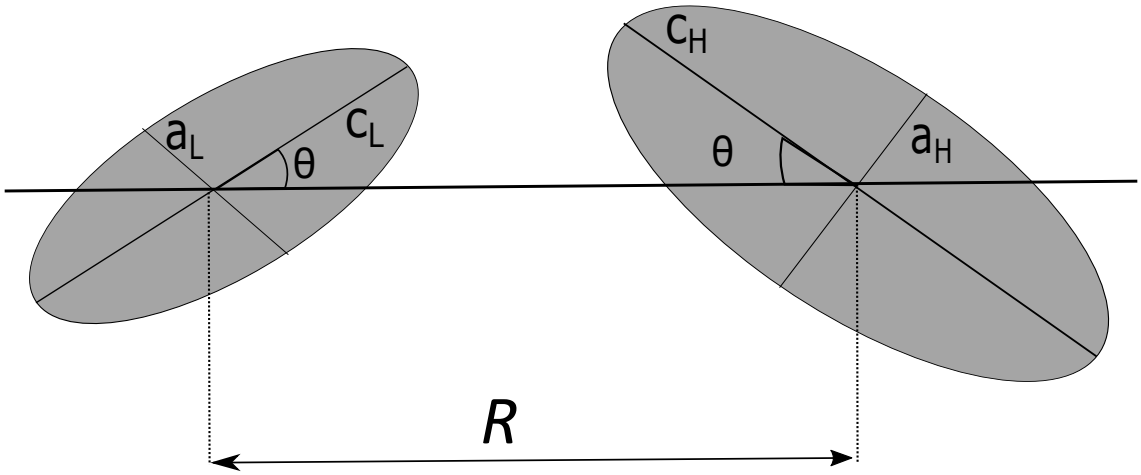

Figure 2.1: Schematic drawing of the DNS in which both fragments have the same orientation angle $\theta_L = \theta_H = \theta$.

tween the major (c_i) and minor (a_i) semiaxis of the nuclei $\beta_i = c_i/a_i$. This definition is suitable up to an axis ratio of ~ 2.1.

The radius of the nucleus is determined by the mass number, and the nucleon radius r_0 by the relationship $R_0 = r_0 A^{1/3}$. For all the nuclei with $Z > 10$, $r_0 = 1.16$ fm; for nuclei with $Z = 2..10$ we use $r_0 = 1.01..1.15$ fm. Considering volume conservation the semiaxis are linked to β by:

$$\begin{aligned} c_i &= r_{0i} A_i^{1/3} \beta_i^{2/3} \\ a_i &= r_{0i} A_i^{1/3} \beta_i^{-1/3}. \end{aligned} \tag{2.1}$$

2.2.2 The interaction energy

Now that we have the means necessary to describe the geometrical properties of the system, we can begin discussing the physical interactions which take place between the two nuclei. Regardless of the approaches or approximations employed, knowledge of the total energy of the system is paramount. The interaction potential of the system is the sum of the Coulomb and nuclear potential and the rotational energy of the system :

$$\begin{aligned} V^{int}(A_i, Z_i, \beta_i, \theta_i, R) \; &= V^C(A_i, Z_i, \beta_L, \beta_H, \theta_L, \theta_H, R) + \\ & V^N(A_i, Z_i, \beta_L, \beta_H, \theta_L, \theta_H, R) + \\ & V^{Rot}(A_i, Z_i, \beta_L, \beta_H, \theta_L, \theta_H, R, l) \end{aligned} \tag{2.2}$$

For the nuclear part the the double folding potential form is used with

Skyrme-type density dependent nucleon forces [5]:

$$V_N = \int \rho_1(\mathbf{r_1})\rho_2(\mathbf{R} - \mathbf{r_2})F(\mathbf{r_1} - \mathbf{r_2})d\mathbf{r_1}d\mathbf{r_2}, \tag{2.3}$$

where $F(\mathbf{r_1} - \mathbf{r_2})$ describes the effective nucleon-nucleon interaction and ρ_i are the nuclear densities (the index $i = 1, 2$ designates the fragments).

For the Coulomb part of the interaction potential Wong's formula [6] is used, and the centrifugal potential will be introduced in Chapter 4.

Analysis of the interaction potential

From an energetic point of view, the minimum of the interaction potential as a function of the orientation of the two fragments is attained for the pole-to-pole orientation. For this reason the azimuthal angles can be ignored, while the polar orientation angles are "frozen" in the pole-to-pole orientation. This configuration greatly simplifies the calculations.

The Coulomb (a-top), nuclear (b-middle) and the total interaction potential (c-bottom) are shown in Figure 2.2 for the nuclear pair ^{106}Mo + ^{146}Ba. The total potential exhibits a local minimum at $d_m \sim 0.5 \pm 0.15$ fm (we will refer to this minimum as a "potential pocket") and a local maximum at $d_B \sim 1.5 - 2$ fm, depending on the mass and charge numbers of the two fragments. The difference between the potential at d_B and d_m is called the quasifission barrier, B_qf and it's an external barrier which hinders the motion of the system in the R coordinates. This allows the system to live in the potential pocket for a sufficiently long time so that statistical equilibrium is achieved. For this reason, the configuration of the system at d_m determines all the important observables: the mass, charge, isotopic and TKE distribution, as well as the spin-, neutron-, and γ-ray multiplicities.

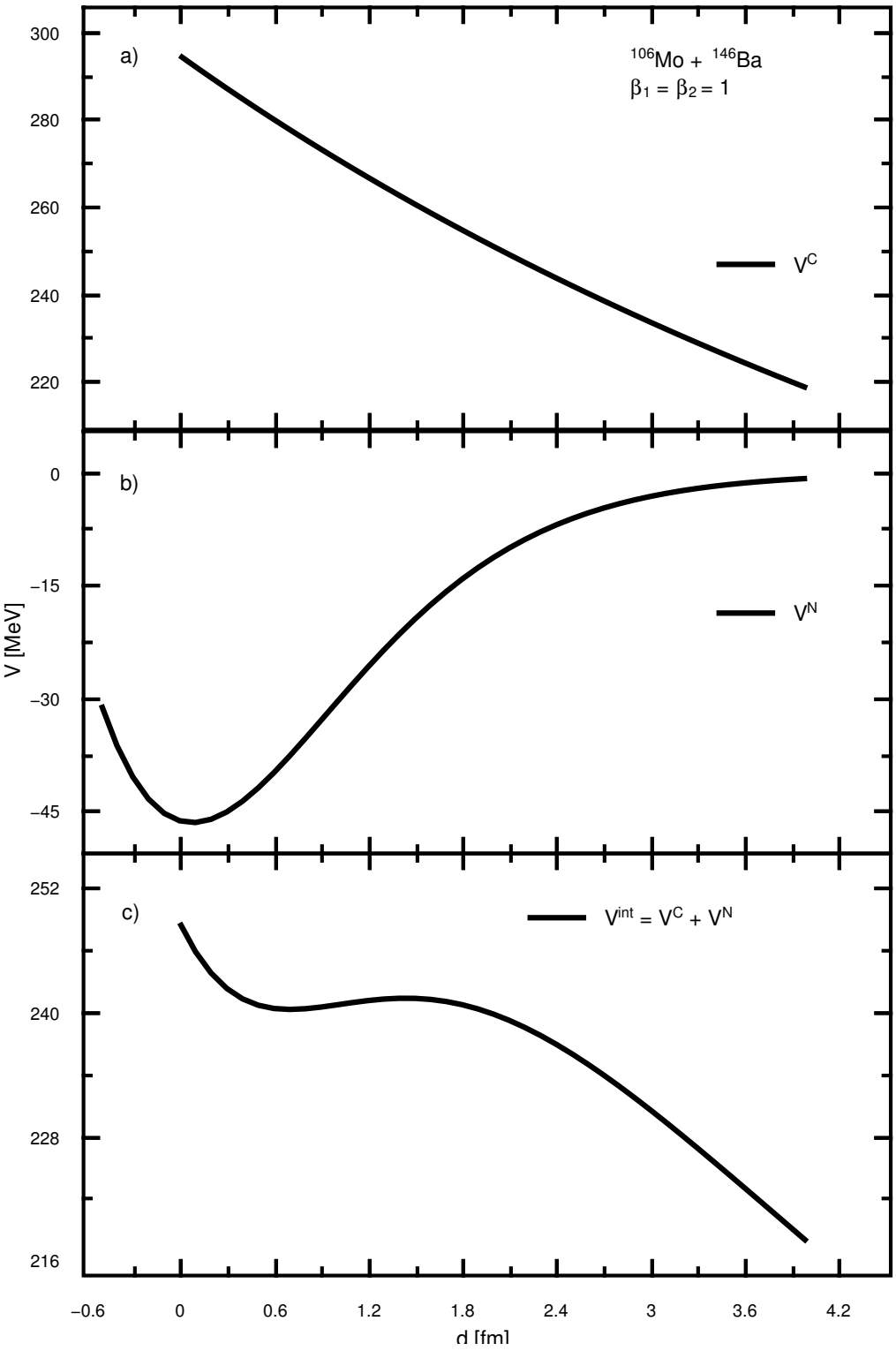

Figure 2.2: The Coulomb (a-top) and the nuclear (b-middle) components of the nuclear potential, and the total interaction potential $V^{int} = V^C + V_N$ calculated for the ^{106}Mo + ^{146}Ba pair. For the sake of simplicity, spherical fragments were considered ($\beta_L = \beta_H = 1$). The distance d is the distance between the nuclear surfaces of the two fragments.

2.2.3 The Liquid Drop energies

The macroscopic part of the binding energy is calculated within the Liquid Drop Model. The main terms are: the surface U^{surf}, Coulomb U^{Coul} and the asymmetry terms.

The surface energy with variable surface tension

The surface energy is proportional to the surface area of each fragment:

$$U^{Surf} = \sigma_i S_i, \tag{2.4}$$

where σ_i is the surface tension coefficient and S_i is the area of the nucleus i.

In order to tackle the problem of deformed nuclei it is usefull to introduce the adimensional parameter B_S, defined by the ratio between the surface the deformed spheriod and the surface of the equvalent sphere [7]::

$$B_S = \frac{S_i}{S_i^0}. \tag{2.5}$$

Restricting ourselves to axially symmetric nucleisimplifies our work, reducing it to the calculation of B_S, which is given by:

$$B_S = \frac{1}{2}\eta^{\frac{2}{3}}\left(1 + \frac{ArcSin(\epsilon)}{\eta\epsilon}\right). \tag{2.6}$$

In Equation(2.6) $\eta = \frac{a}{c}$ is the inverse of the deformation parameter β defined in Chapter 2.2.1, and $\epsilon = \left(1 - \eta^2\right)^{1/2}$ is the eccentricity. [7] .

If one uses a constant value for σ, then the moments of inertia of fissioning nuclei are larger than the experimental one [3]. Here we avoid this drawback, while remaining within the LDM, by using a deformation dependent surface tension coefficient $\sigma_i = \sigma_i(\beta)$:

$$\sigma_i(\beta_i) = \sigma_{0,i}(1 + k_i(\beta_i - \beta_i^{g.s.})^2) \tag{2.7}$$

with [9]:

$$\sigma_{0,i} = 0.9517(1 - 1.7826((N_i - Z_i)^2)/A_i)^2), \tag{2.8}$$

and $\beta_{g.s.}$ are the ground state deformations, taken from refs.[10, 11, 12]. The surface tension coefficient is taken as:

$$k_i = \frac{1}{1 + Exp\left[-0.063(C_{vib}(Z_i, A_i) - 67)\right]}, \tag{2.9}$$

where C_{vib}, in units of MeV, is the stiffness of the nucleus [13]. The stiffness parameter was determined in [4]:

$$C_{vib}(A_i, Z_i) = \frac{\hbar\omega^i_{vib}\left(3Z_i e R^2_{0,i}/\left(4\pi\right)\right)}{2B\left(E_2\right)^i_{vib}} \tag{2.10}$$

where:

$$2B\left(E_2\right)^i_{vib} \simeq \frac{E^i_{2+}B(E2)^i_{rot}}{\hbar\omega^i_{vib}} \tag{2.11}$$

E^i_{2+} is the energy of the fist 2^+ state. The 2^+ states are assumed to be vibrational ones.

The Liquid-Drop Coulomb and symmetry energy

The Coulomb energy of a uniformly charged ($q = Ze$) sphere of radius R_0 can be written [7]:

$$U^{Coul,0}_i = \frac{3e^2}{5r_0}\frac{Z^2_i}{A^{1/3}_i}. \tag{2.12}$$

Using the same logic as in the deduction of the surface energy, we can define a deformation Coulomb energy as the ratio between the energy of a uniformly charged spheroid and that of a sphere [7]:

$$B_C = \frac{1}{2}\frac{\eta^{\frac{2}{3}}}{\epsilon} ln\left(\frac{1+\epsilon}{1-\epsilon}\right). \tag{2.13}$$

The parameters ϵ and η have the same meaning as in Equation(2.6). The symmetry energy is taken as:

$$U^{sym}_i = 27.612\frac{(A_i - 2Z_i)^2}{A_i}. \tag{2.14}$$

2.2.4 Shell corrections

In [15, 16, 17] Strutinski approximates the influence of the shell structure on the binding energy as a small deviation from a uniform nucleon distribution. Under these circumstances the shell corrections are defined as:

$$\delta U = \sum_{\nu} E_{\nu} - \widetilde{U}, \tag{2.15}$$

where E_ν are the nucleon energies calculated within a shell-model and $\widetilde{U}$ is:

$$\widetilde{U} = \int_{-\infty}^{\widetilde{\lambda}} E\widetilde{g}(E)dE, \tag{2.16}$$

where $\widetilde{g}$ is called the uniform distribution function.

The Strutinski prescription allows total freedom upon which single-particle model is to be used. In the current work we use the two-center shell model of [19, 9]. More details are given in the Thesis and in the reference [19].

2.3 The potential energy surface (PES)

We now have all the ingredients necessary to calculate the total potential energy of the system, which takes the form:

$$\begin{aligned} U(A_i, Z_i, \beta_i, R) &= U_L^{LD}(A_L, Z_L, \beta_L, E_L^*) + \delta U_L^{shell}(A_L, Z_L, \beta_L, E_L^*) \\ &+ U_H^{LD}(A_H, Z_H, \beta_H, E_H^*) + \delta U_H^{shell}(A_H, Z_H, \beta_H, E_H^*) \\ &+ V^C(A_i, Z_i, \beta_i, R_m) + V^N(A_i, Z_i, \beta_i, R_m). \end{aligned} \tag{2.17}$$

In the above equation

$$U_i^{LD}(A_i, Z_i, \beta_i) = U_i^{sym}(A_i, Z_i) + U_i^C(A_i, Z_i, \beta_i) + U_i^{Surf}(A_i, Z_i, \beta_i) \tag{2.18}$$

is the sum of the the LDM energies (i.e. the binding energy), δU_i^{shell} is the shell correction of the fragment i, $V^C + V^N$ is the interaction energy and E^* is the excitation energy.

It is easy to see that, even though we were able to reduce the number of variables, U still remains a complex function. The variation of the total energy of the system with the mass, charge and deformation parameters is of the utmost importance, as it describes the evolution of the system. For us it

is convenient to calculate the PES as a function of the deformation parameters β_1 and β_2, because it gives a visual representation of the configuration of the system at the moment of scission.

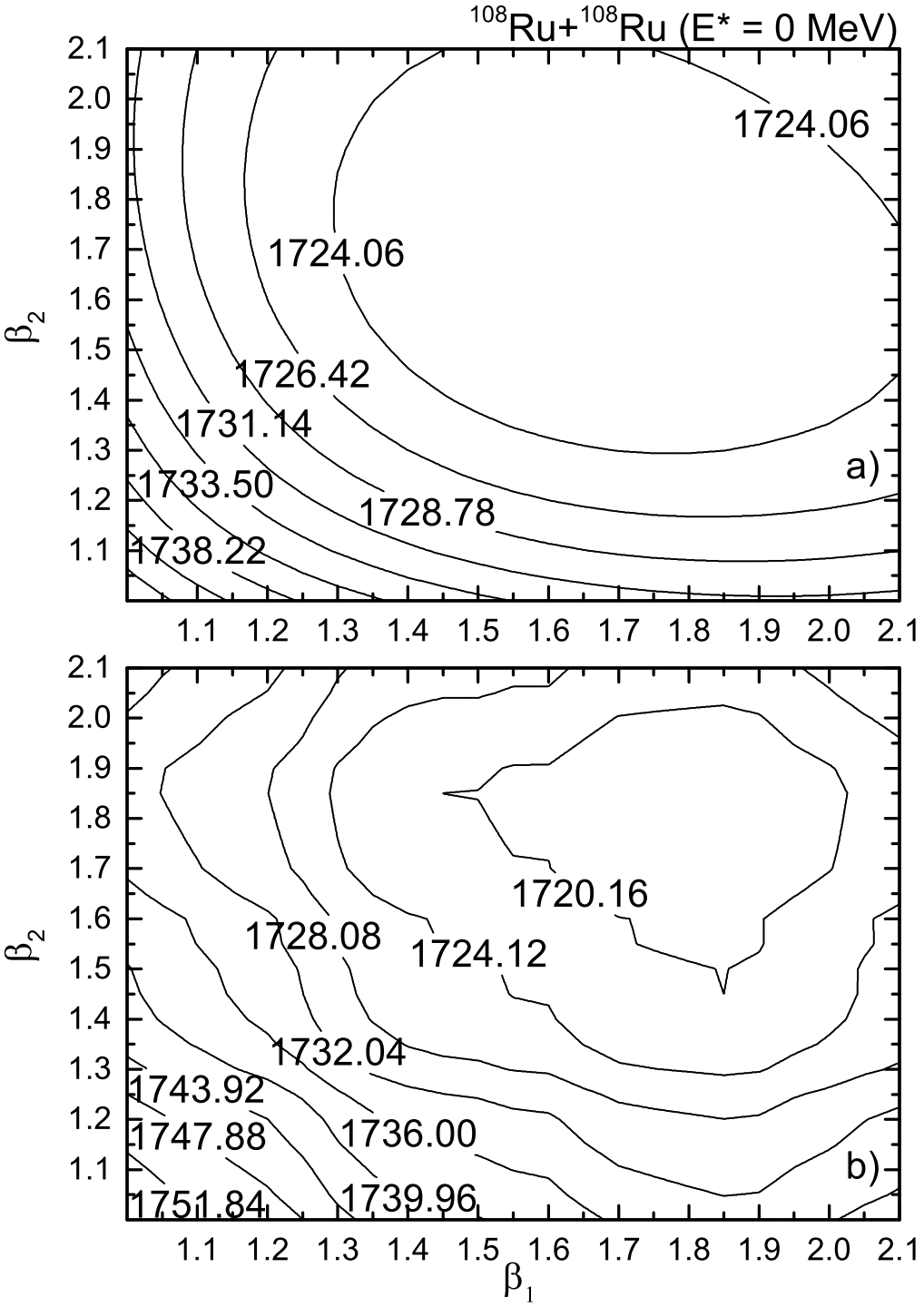

Figure 2.3: Potential energy sufraces for the symmetric DNS ^{108}Ru+^{108}Ru, without shell corrections (top) and with shell corrections (bottom). The excitation energy of the system is zero. The values are in units of MeV.

Such a PES is shown in Figure (2.3), without the shell corrections (a)-top) and with the shell corrections (b)-bottom). In the upper part of the figure one can see that a relatively wide minimum appears at large deformations. The minimum appears as the result of two competing energies - the interaction potential, which decreases fast with increasing deformation, and the LDM energies, or more exactly, the surface energy, which increases with deformation. The position of the minimum in the PES points to the most favourable deformations at the moment of scission. One can easily notice that these deformations are much larger than the ground-state ones. Also it is easily observable that the shell corrections can bring major changes to the PES, by shrinking or "moving" the minima, or can even lead to the formation of secondary minima.

2.3.1 The excitation energy and its effects

A mononucleus can spontaneously undergo fission if, and only if, the energy of the scission configuration is smaller than the energy of the initial CN. Due to the conservation laws, the system accumulates a considerable amount of excitation excitation E^* energy on its way to the fission path.

The excitation energy is calculated, based on the conservation of energy, as the sum of the initial excitation energy of the nucleus $E_0^* = E_{n,\gamma} + Q_n$ plus the difference between the potential energies of the fissioning nucleus $U_{C.N.}(A, Z, \beta)$ and the dinuclear system at the scission point $U(A_i, Z_i, \beta_i, R_m)$ [8]:

$$E^*(A_i, Z_i, \beta_i, R_m) = E_0^* + Q - V^{int}\left(\left\{A_i, Z_i, \beta_i^{g.s.}\right\}, R_m\right) + \left[U\left(\{A_i, Z_i, \beta_i\}, R_m, E^*\right) - U\left(\left\{A_i, Z_i, \beta_i^{g.s.}\right\}, R_m, E^*\right)\right]. \quad (2.19)$$

The term $E_{n,\gamma}$ is the energy of the bombarding neutron (gamma quanta) in the case of neutron (photo) induced fission and Q_n is the reaction heat. In the case of spontaneous fission $E_0^* = 0$, in the case of the electromagnetic induced fission it is equal to the energy of the γ cuanta ($E_{C.N.}^* = E_\gamma$), and in the case of thermal neutron induced fission $E_0^* \sim 6 - 8$ MeV.

Because of the intimate connection between the excitation energy and the total potential energy of the system, E^* varies with deformation.The excitation energy has a maximal value at the deepest point of the PES.

Typical values are $E^* = 10 - 15$ MeV for the spontaneous fission of actinides and $E^* = 15 - 25$ MeV for the neutron induced fission of actinides. For such high energies the shell structure of the nucleus is disrupted, and the shell correction to the binding energy needs to be dampened. In [20] a phenomenological expression was used:

$$\delta U_i^{shell}(A_i, Z_i, \beta_i, E_i^*) = \delta U_i^{shell}(A_i, Z_i, \beta_i, E_i^* = 0) \exp[-E_i^*/E_D], \quad (2.20)$$

with $E_D = 18.5$ MeV. In Equation(2.20) E_i^* is the excitation energy of the ith fragment. The excitation energy of the system is assumed to be shared between the fragments proportional to

$$E_i^* = E^* \frac{A_i}{A_{CN}}. \quad (2.21)$$

On the basis of a Hartree-Fock method, [25] the Coulomb, surface, and symmetry LDM terms were found to exhibit a temperature dependence as well. We use the same dependence type as in [25], but with a different set of parameters:

$$U_i^{sym}(A_i, Z_i, E^*) = U_i^{sym}(A_i, Z_i, T = 0)(1 + 6 \times 10^{-4} E_i^*/A_i),$$

$$U_i^{Coul}(A_i, Z_i, \beta_i, E^*) = U_i^{C}(A_i, Z_i, \beta_i, T = 0)(1 - 0.12 E_i^*/A_i),$$

$$U_i^{Surf}(A_i, Z_i, \beta_i, E^*) = U_i^{Surf}(A_i, Z_i, \beta_i, T = 0)(1 + 0.102 E_i^*/A_i). \quad (2.22)$$

$$r_0(E_i^*) = r_0(E_i^* = 0)\left(1 + 5.04 \times 10^{-3} E_i^*/A_i\right). \quad (2.23)$$

The Equation (2.23) describes the expansion of the nuclear matter, and it simultaneously explains the increase in the surface energy through the increase of the area, and the decrease of the Coulomb energy through the increase of the volume of the nuclei.

The damping of the stiffness parameter with excitation energy E_i^* is introduced as:

$$k_i(E_i^*) = k_i * exp\left[-E_i^*/E_k\right], \quad (2.24)$$

with $E_k = 3.7$ MeV.

The temperature of the decaying system is related to the excitation energy by:

$$T = \sqrt{E^*/a}, \quad (2.25)$$

where a is the level density parameter in the Fermi-gas model. For the present calculations we chose the value $a = A/12$ MeV $^{-1}$ which was used for the description of fusion [42, 43, 44, 45, 46].

2.4 The statistical scission-point model

In an ample study [26], it was proven that the relative formation probability of the DNS with particular masses, can be calculated as:

$$W(A_i, Z_i, \beta_i, E^*) = N_0 \exp\left[-\frac{U\left(\{A_i, Z_i, \beta_i\}, R_m\right)}{T}\right], \tag{2.26}$$

where N_0 is a normalization factor. The same conclusion can be achieved within a transport model. For example, Kalandarov et. al. [27, 28, 29] calculated the time dependence of the probability $P_{Z,A}(t)$ of finding a system at the moment t in a state with the mass and charge number Z and A by starting from a master equation:

$$\begin{aligned}\frac{d}{dt}P_{Z,A}(t) &= \Delta^{(-,0)}_{Z+1,A+1}P_{Z+1,A+1}(t) + \Delta^{(+,0)}_{Z-1,A-1}P_{Z-1,A-1}(t) \\ &+ \Delta^{(0,-)}_{Z,A+1}P_{Z,A+1}(t) + \Delta^{(0,+)}_{Z,A-1}P_{Z,A-1}(t) \\ &- \left[\Delta^{(0,-)}_{Z,A} + \Delta^{(0,+)}_{Z,A} + \Delta^{(-,0)}_{Z,A} + \Delta^{(+,0)}_{Z,A}\right]P_{Z_A}(t),\end{aligned} \tag{2.27}$$

with the innitial condition $P_{Z_A}(t = 0) = \delta_{Z,Z_{C.N.}}\delta_{A,A_{C.N.}}$. The terms $\Delta^{(\pm,0)}$ characterize the proton transport rates while $\Delta^{(0,\pm)}$ describes the neutron transport rates. The transport coefficients are time independent, which guarantees the existence of a stationary solution $P_{Z,A}(t \to \infty) = P_{Z,A}(E^*)$.

We have stated earlier that the system is trapped inside the potential pocket, where it lives for a sufficiently long time. The probability that the system thermally overcomes the quasifission barrier B_{qf} is taken from the transition state theory [30] in the limit of high temperature:

$$P^{decay}_{Z_i,A_i,\beta_i,R} \sim \exp\left[-\frac{B_{q.f.}\left(\{A_i, Z_i, \beta_i\}, R\right)}{T}\right]. \tag{2.28}$$

In this sense, the binary decay can be seen as a two-step process. At first the system undergoes a motion in the mass and charge coordinates, under the influence of the potential $U\left(\{A_i, Z_i, \beta_i\}, R_m\right)$ -hence the name "driving potential"; the newly-formed DNS, settles into the potential pocket, and its isotopic composition is fully described by Equation(2.26). The second step is a large amplitude motion in the disintegration coordinate R. It can only take place if the excitation energy of the DNS is large enough to overcome the barrier. Thus, we can write the total emission probability as the product of the formation and decay probabilities:

$$w(A_i, Z_i, \beta_i, E^*) = N_0 \exp\left[-\frac{U(A_i, Z_i, \beta_i, R_m) + B_{qf}(A_i, Z_i, \beta_i)}{T}\right]. \tag{2.29}$$

In order to obtain the mass-charge distribution of fission fragments, one should integrate (2.29) over β_L and β_H:

$$Y(A_i, Z_i, E^*) = N_0 \int d\beta_L d\beta_H w(A_i, Z_i, \beta_i, E^*). \tag{2.30}$$

To obtain the mass (charge) distribution one should sum over the charge (mass) numbers of the fragments:

$$Y(A_i) = N_0 \sum_{Z_i} \int\int w(A_i, Z_i, \beta_1, \beta_2, E^*)\, \mathrm{d}\beta_1 \mathrm{d}\beta_2, \tag{2.31}$$

$$Y(Z_i) = N_0 \sum_{A_i} \int\int w(A_i, Z_i, \beta_1, \beta_2, E^*)\, \mathrm{d}\beta_1 \mathrm{d}\beta_2, \tag{2.32}$$

The statistical model, in the form presented so far, predicts a high maxima of the mass/charge distribution at symmetry in the cases of ^{235}U(n,f) and ^{239}Pu(n,f), as opposed to the experimental data. To overcome this, the author proposes a restriction on the integration limit in Equations (2.31) and (2.32) as described below [21]-[24]. Practically speaking, above a certain deformation, the quasifission barrier diminishes considerably and can not contain the system. In this work are taken into account only those configurations for which $B_{qf} > 0.7 - 1$ MeV depending on the charge number of the fissioning nucleus. These values provide a good description with the experimental data as we will show [21]-[24]. .

Due to the excitation energy of system, the fission fragments can evaporate several prompt neutrons. This does not change the charge distribution, but it changes the mass number of the final fragments. Thus, in order to compare the experimental mass or isotopic distributions with the calculated ones, one needs to correct the theoretical results by subtracting the number of emitted neutrons from the initial masses. To calculate the neutron multiplicity distributions the following expression was used:

$$< n_i >= \frac{E_i^{'*}}{B_{ni} + 2T_i}. \tag{2.33}$$

The term B_{ni} is the separation energy of the first neutron, and the term $2T_i$ is included to describe the kinetic energy of the evaporated neutron [3]. Since the fragments are deformed at scission, the relaxation of the deformations to the ground state values increases the excitation energy of the nucleus by an amount equal to the deformation energy:

$$E_i^{'*} = E^* \frac{A_i}{A_1 + A_2} + E_i^{def}, \tag{2.34}$$

where $E_i^{def} = \Big(U_i^{LD}(\beta_i) + \delta U_i(\beta_i)\Big) - \Big(U_i^{LD}(\beta_i^{g.s.}) + \delta U_i(\beta_i^{g.s.})\Big)$.

Another important characteristic of fission is the total kinetic energy $TKE = V^C + V^N$ of the final fragments. Within the statistical model, we can write the TKE as a function of the mass number as:

$$\begin{aligned} &<TKE>(A_i) = \\ &= \frac{\sum_{Z_i} TKE(A_i, Z_i, \beta_1^{min}, \beta_2^{min})\, w(A_i, Z_i, \beta_1^{min}, \beta_2^{min}, E^*)}{\sum_{Z_i} w(A_i, Z_i, \beta_1^{min}, \beta_2^{min}, E^*)}. \end{aligned} \tag{2.35}$$

or as function of the charge number:

$$\begin{aligned} &<TKE>(Z_i) = \\ &= \frac{\sum_{A_i} TKE(A_i, Z_i, \beta_1^{min}, \beta_2^{min})\, w(A_i, Z_i, \beta_1^{min}, \beta_2^{min}, E^*)}{\sum_{A_i} w(A_i, Z_i, \beta_1^{min}, \beta_2^{min}, E^*)}. \end{aligned} \tag{2.36}$$

The average value of TKE of the fission fragments can be found by averaging over all binary systems:

$$\overline{TKE} = \sum_{Z_i, A_i} TKE(A_i, Z_i) Y(A_i, Z_i, E^*). \tag{2.37}$$

Results: the mass, charge, isotopic and TKE distributions

3.1 The charge and mass distributions at fixed energies

In Figures (3.1) – (3.4) the theoretical charge distributions (solid lines) [21] are compared with the experimental data of [32] (solid symbols) for the electromagnetic induced fission (E_γ = 11 MeV) of the indicated nuclei. The calculations are done for even-even pair of nuclei. Although in some cases the eve-odd effects are noticeably present, they can not change the shape of the distribution in any significant way. Also for the majority of the reactions studied in this work, the number of pre-scission neutrons is ~ 0, and their effect is safely neglected.

As can be seen, our model is well suited for the description of both symmetric and asymmetric description, showing a very good agreement with the experimental data. For the induced fission of Rn, Ra and $^{218-222}$Th nuclei, the distribution is symmetrical, with a single prominent peak around $Z_{C.N.}/2$. In the case of $A = 224$ thorium, the distribution exhibits the start of the formation of asymmetric maxima, and for the $A = 226$ the yields of Kr–Sr, and of their complementary fragments, are equal to those of Pd–Ru. As the mass number increases, the asymmetric fission mode becomes dominant. The author points-out that the central maximum doesn't immediately disappear; it still exists, although it's 2-3 times smaller than the asymmetric ones. In the case of ^{230}U (Figure 3.4), there are no clear signs of a central maximum, although the odd-even effects are strong at symmetry. For the uranium isotopes with $A \geq 232$ the symmetric yields are almost zero, and the asymmetric nature of the distribution is evident.

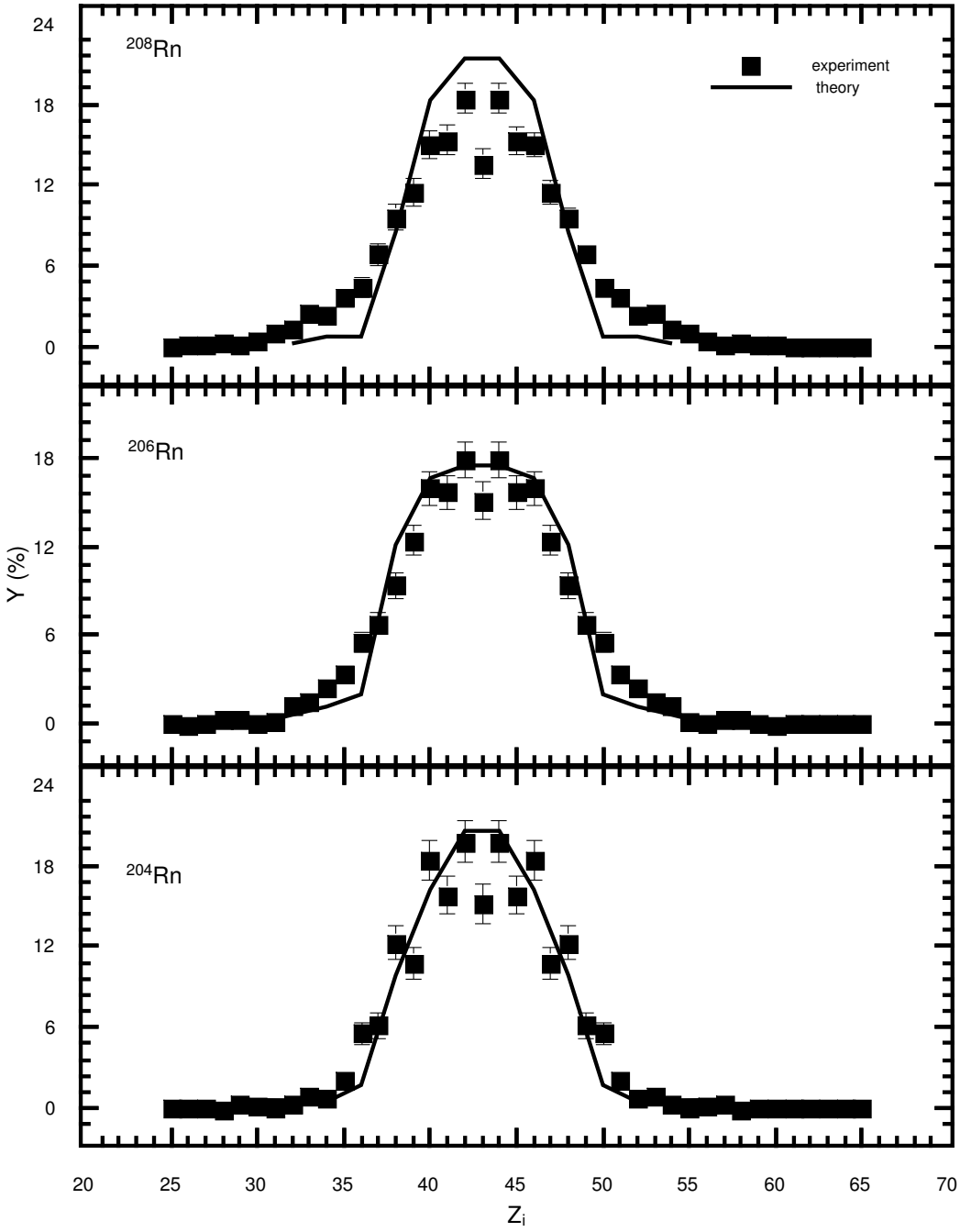

Figure 3.1: The calculated charge distributions (lines) for electromagnetic-induced fission of the indicated radon and uranium isotopes at 11 MeV excitation energy are compared with the experimental data [32] (symbols). The lines connect the calculated points for even-even fission fragments.

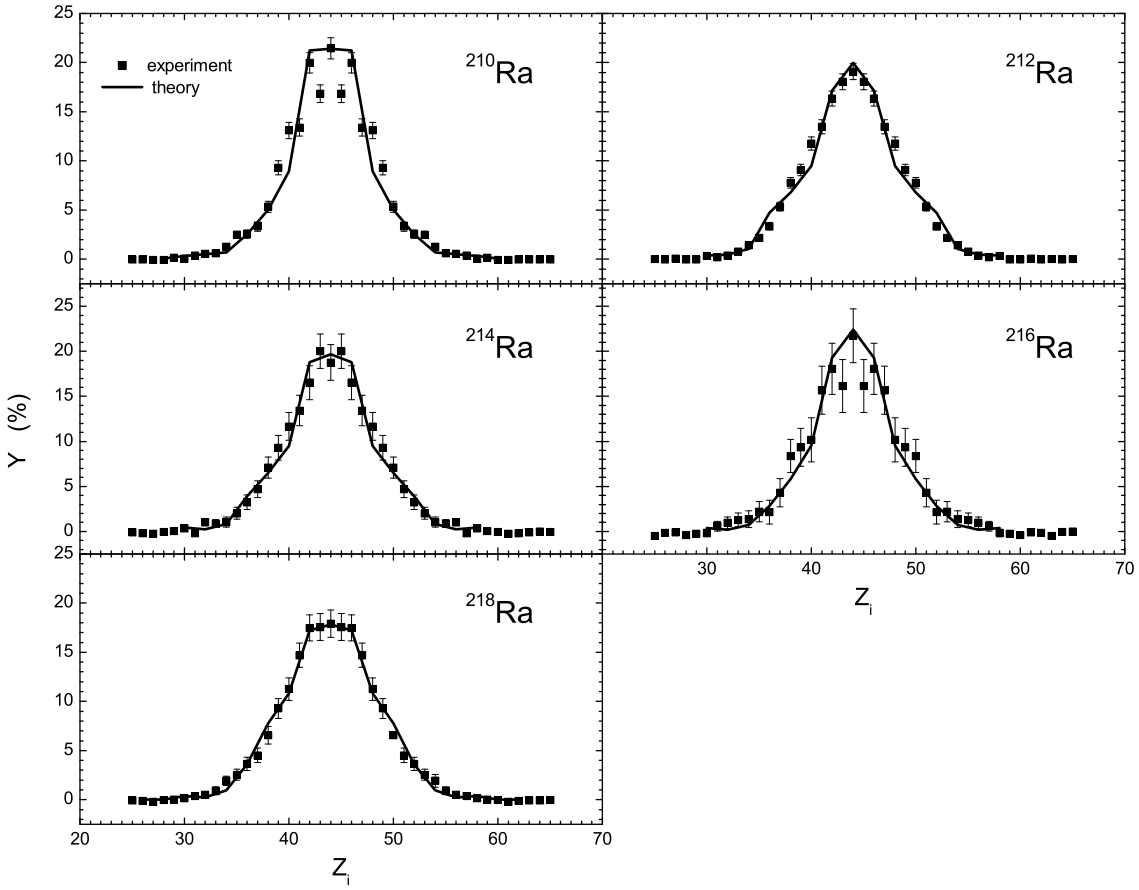

Figure 3.2: The same as in Figure 3.1, but for the indicated radium isotopes.

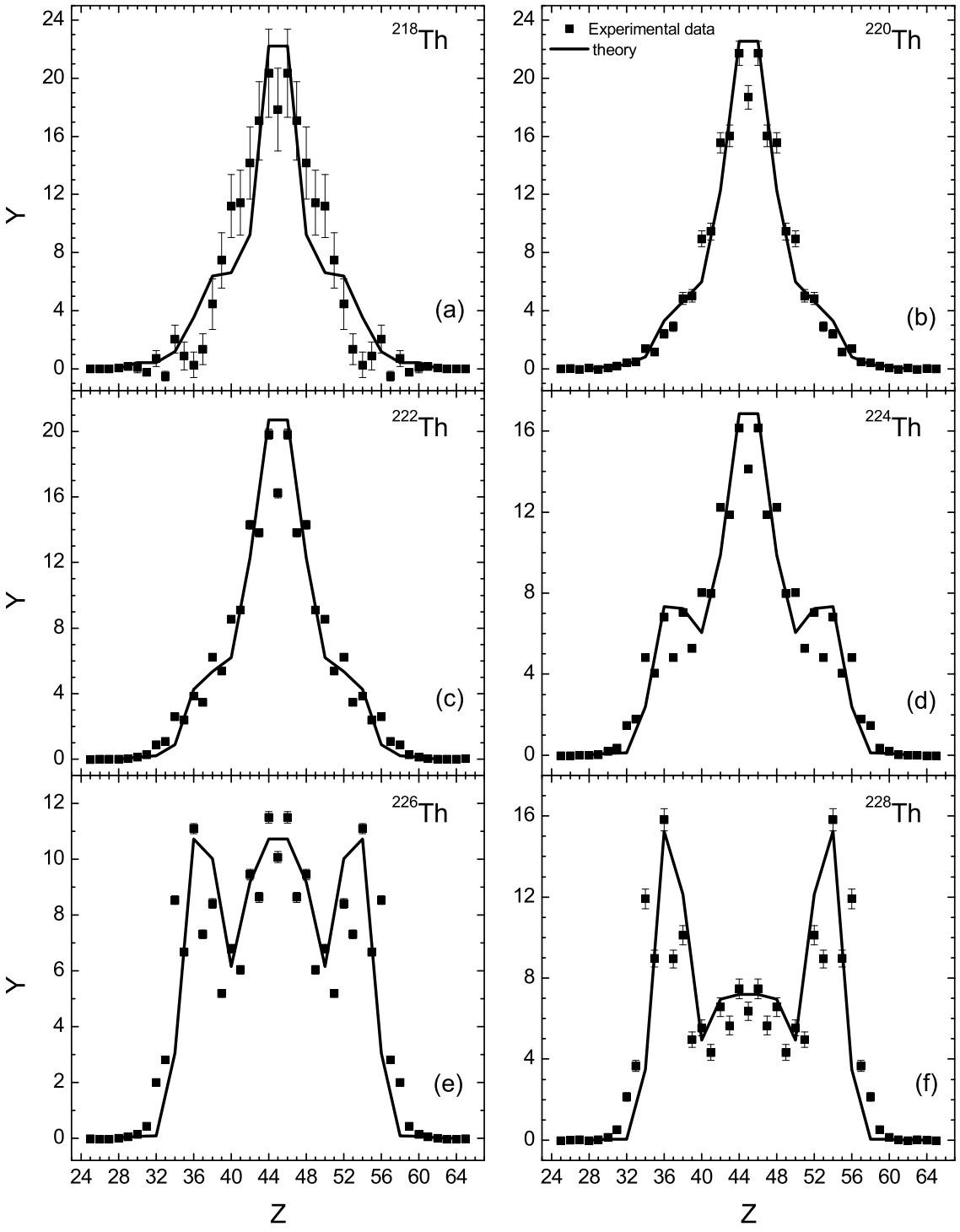

Figure 3.3: The same as in Figure 3.1, but for the indicated thorium isotopes.

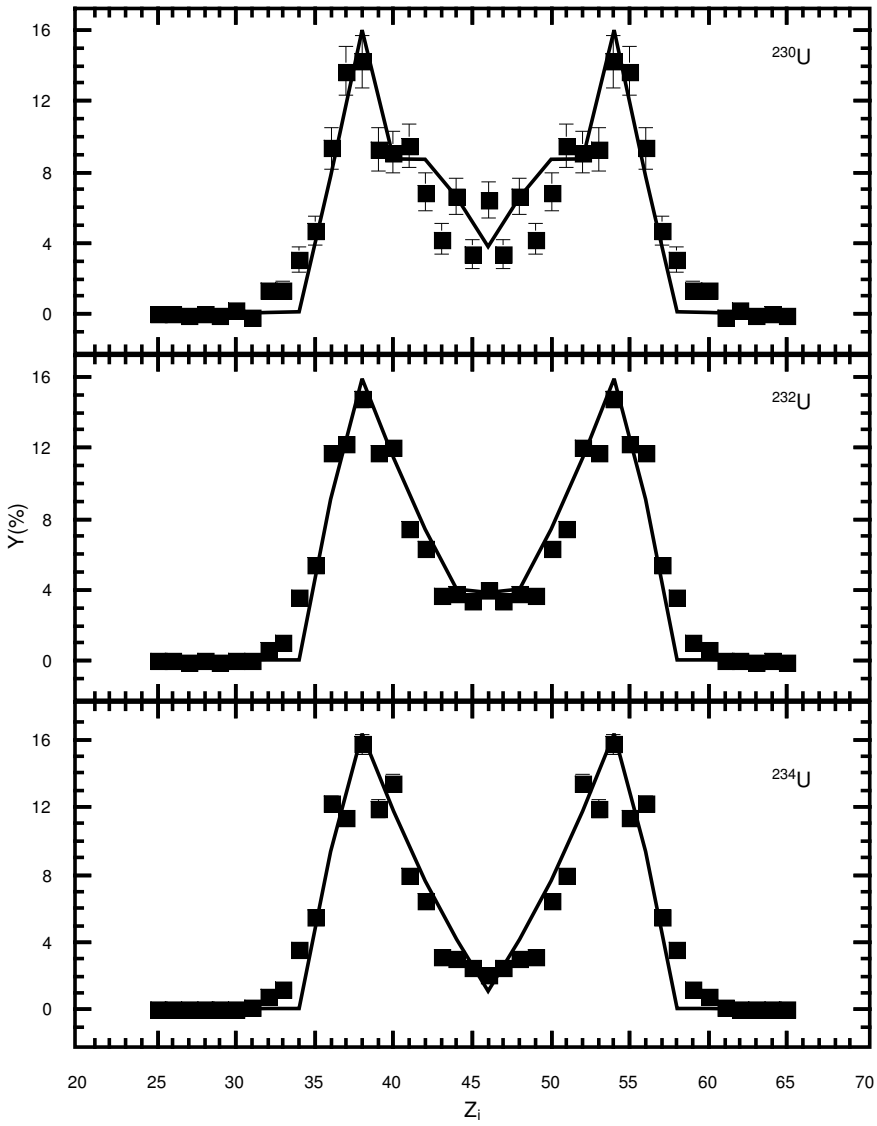

Figure 3.4: The same as in Figure 3.1, but for the indicated uranium isotopes.

3.2 The evolution of the charge and mass distributions with excitation energy

In Ref. [34], the competition between symmetric and asymmetric fission was suggested to be related to the shell effects in the deformed fissioning nucleus. With increasing energythe shell effects are supposed to be washed out, leaving the nucleus with a dominant symmetric mode of fission. The new experimental data regarding ^{180}Hg [35, 36], however, show that the

asymmetric mass distribution can not be explain by the microscopic effects alone.

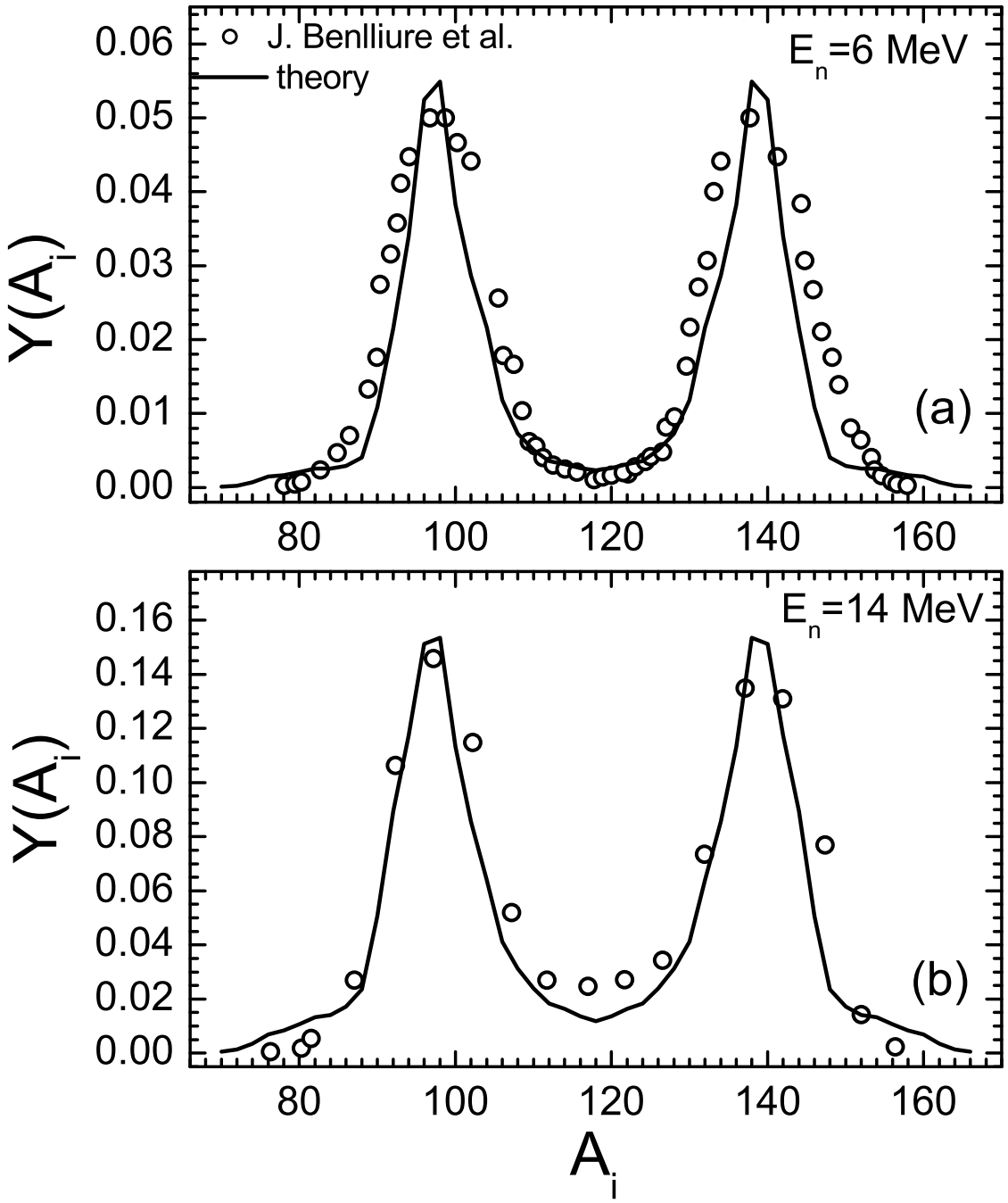

Figure 3.5: The calculated mass distributions (solid lines) for fission of ^{235}U by neutrons with incident energies 6 MeV (a) and 14 MeV (b). The experimental data (symbols) are from Ref.[38].

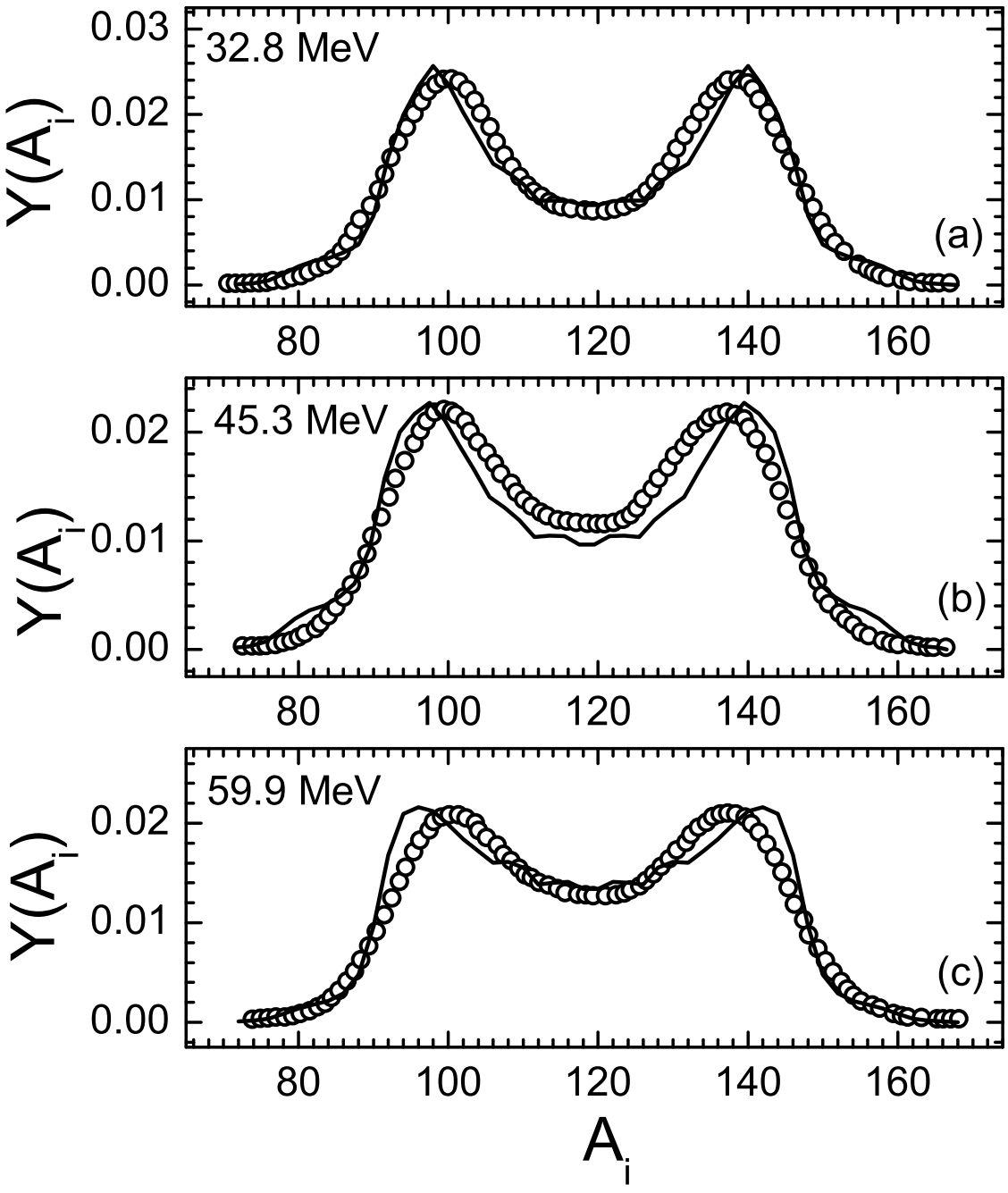

Figure 3.6: The calculated fragment mass distribution (solid lines) is compared with the experimental data [37] for the ^{238}U(n,f) reaction at indicated incident neutron energies 32.8 (a), 45.3 (b), and 59.9 (c) MeV.

The fission-fragment mass yields for the neutron-induced fission of ^{232}Th and ^{238}U at high energies ($E_n > 30$ MeV) have been recently measured. The experimental results [37] demonstrated that the probability of symmetric fission increases with incident neutron energy for both nuclei, but the distribution maintains it's a asymmetric shape.

The theoretical mass distribution in the case of 6 and 14 MeV neutron induced fission of ^{235}U is compared with experimental data [22] and shown in Figure 3.5, while in Figure 3.6, the calculated and experimental results of the 32.8, 45.3 and 59.9 MeV neutron induced fission of ^{238}U are presented.

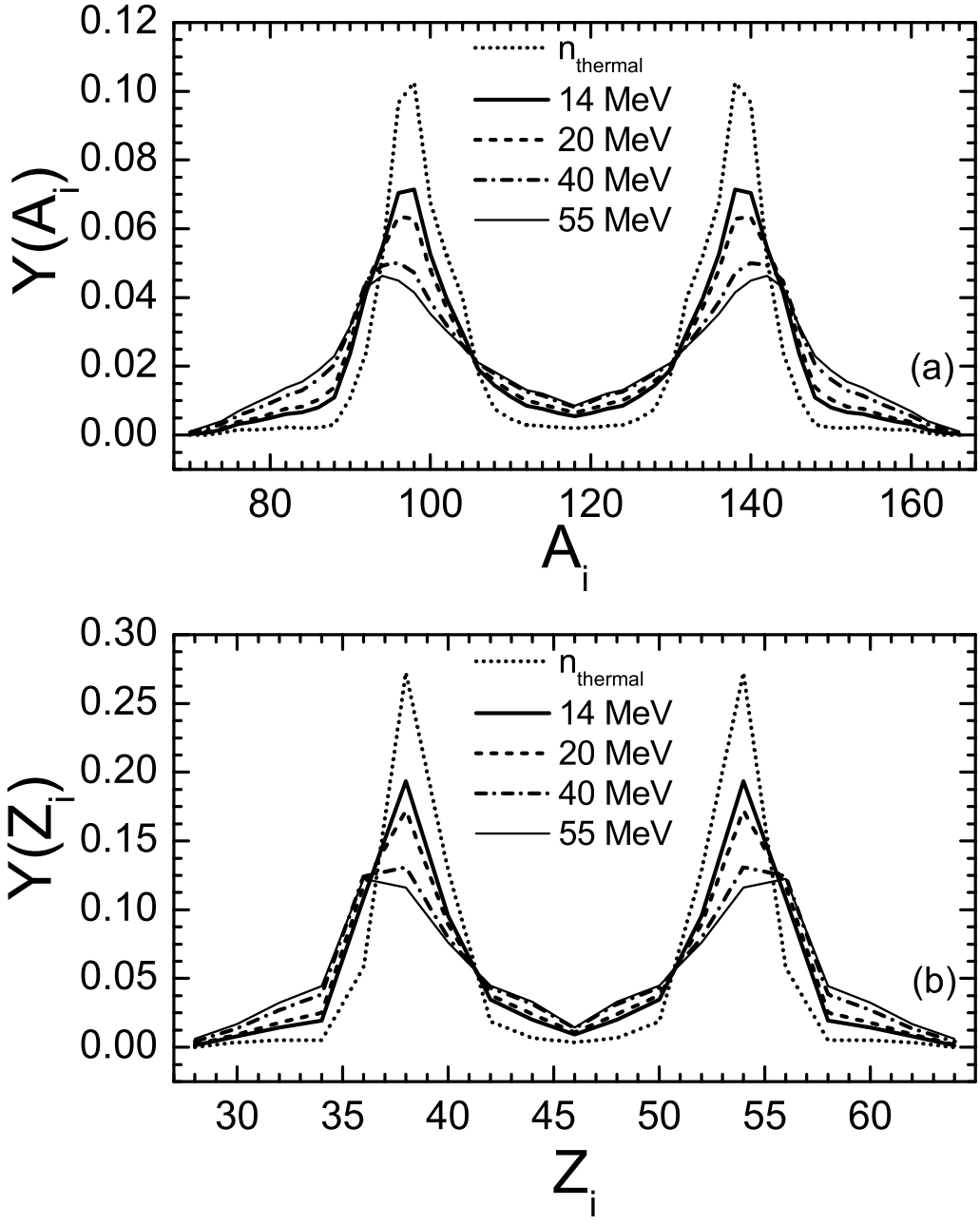

Figure 3.7: The calculated fragment mass (a) and charge (b) distributions in the ^{235}U(n,f) reaction at the incident neutron energies indicated. The calculations were performed for even-Z_i fragments. The calculations were performed for even-Z_i fragments.

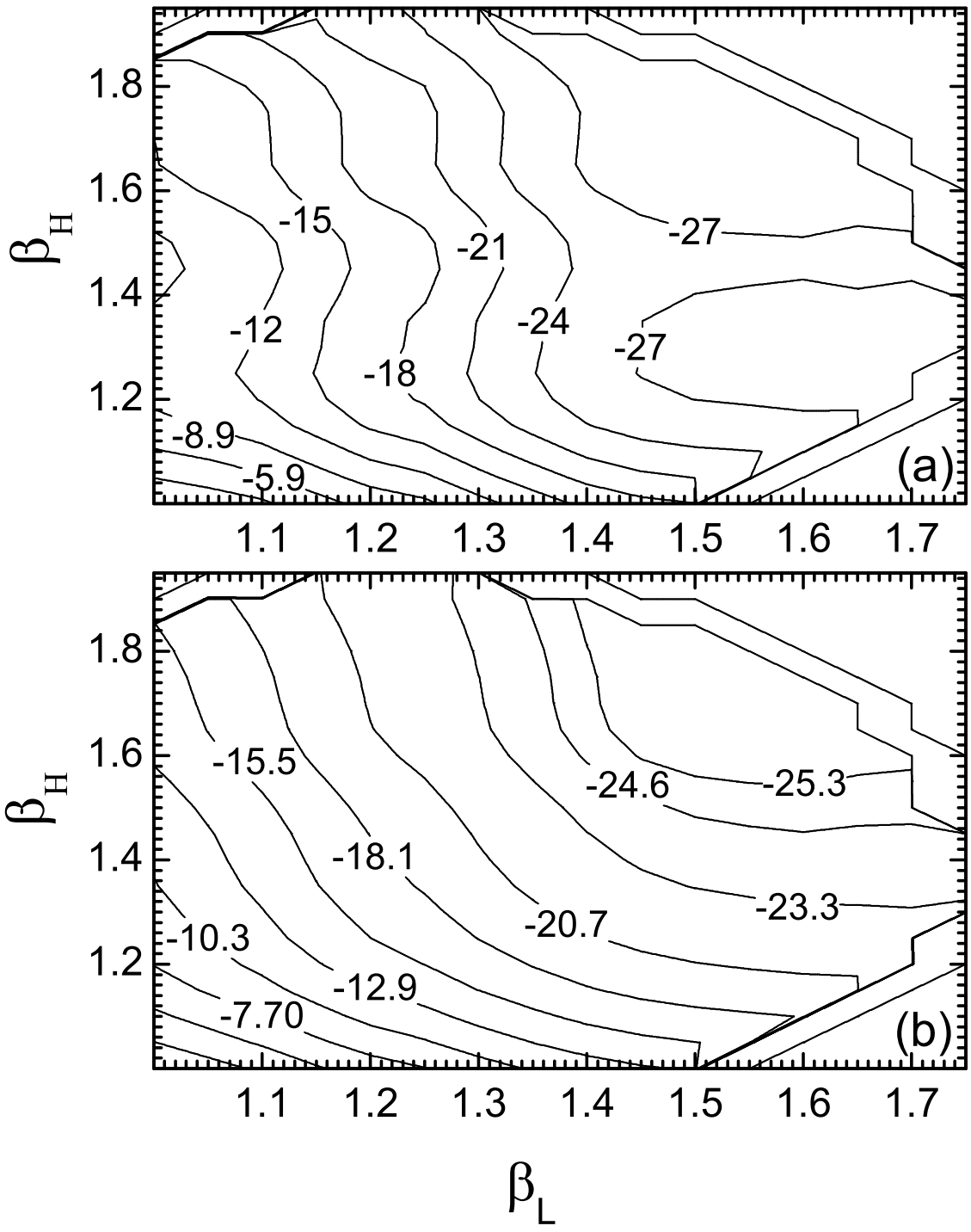

Figure 3.8: The calculated potential-energy surfaces (in MeV) for the DNS with $(A_L, Z_L) = (96, 36)$ and $(A_H, Z_H) = (140, 56)$ at $E_n = 0$ MeV (a) and $E_n = 55$ MeV (b). The value of potential energy is normalized to the energy of the DNS with the spherical nuclei ($\beta_L = \beta_H = 1$). In the nuclear shape parametrization used, the value of the quadrupole deformation parameter is approximately $\beta_i - 1$ ($i = L, H$).

To study the influence of the bombarding energy on the isotopic, mass and charge distributions the reaction ^{235}U(n,f), E_n = 14, 20, 40 și 55 MeV (Figure 3.7) was considered. The conservation of the asymmetric shape is predicted.

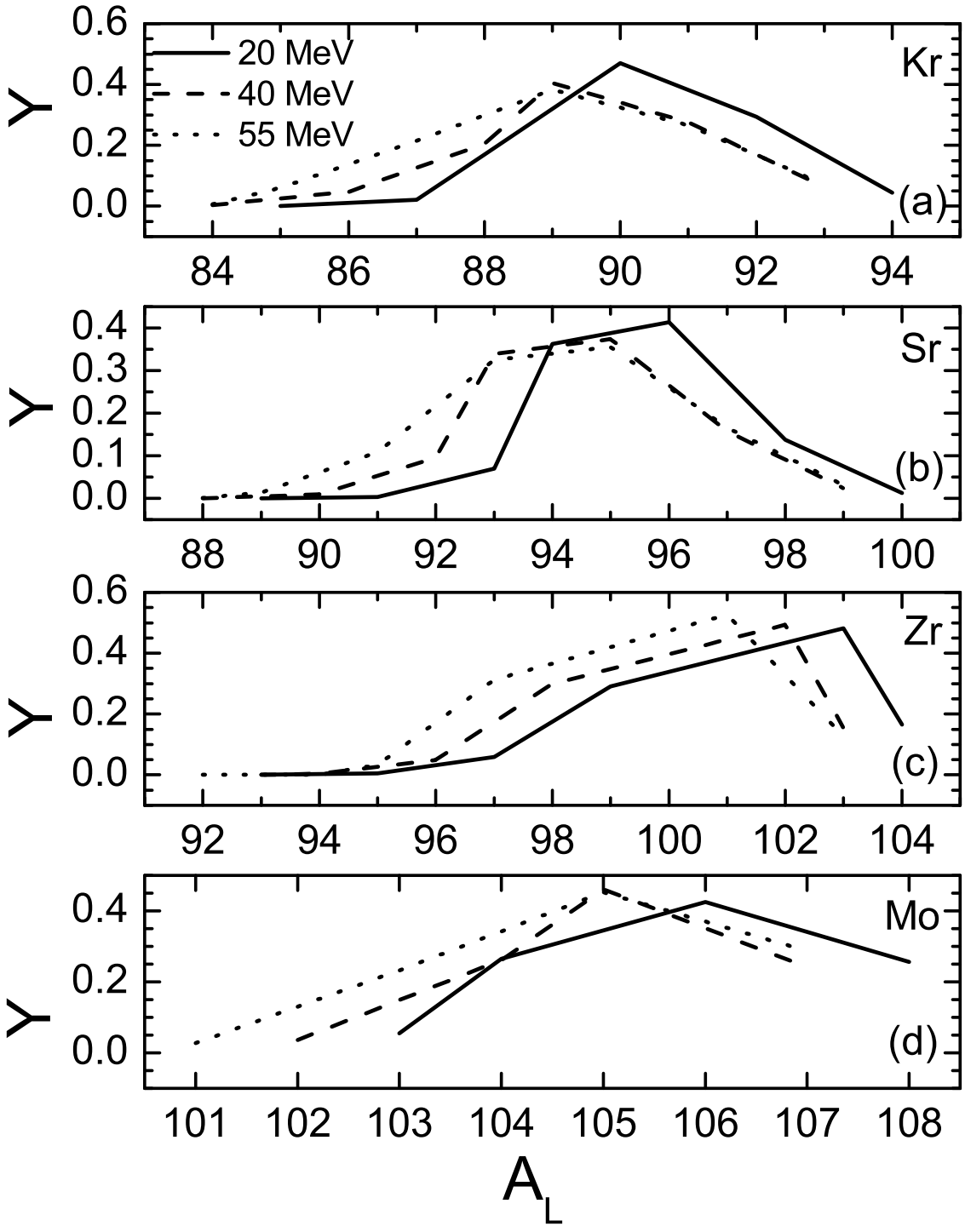

Figure 3.9: The calculated isotopic trends for the nuclei Kr (a), Sr (b), Zr (c), și Mo (d) in the reaction ^{235}U(n,f) at the indicated neutron energies.

The results point out to the fact that the structures present in the PEs govern the emission of the fission fragments. The excitation energy reduces the shell effects and the rigidity of the nuclear surface, which leads to a widening of the minima in the deformation plane (Figure 3.8).

In Figure 3.9 is predicted the isotopic distribution of the fragments $Z = 36, 38, 40, 42$ at different bombarding energies. The only notable changes are the shifting of the maxima towards smaller neutron number. This fact is easily explainable on the basis that at larger excitation energies the number of the primary emitted neutrons is larger.

3.2.1 Unexpected charge asymmetry of thorium isotopes at high excitation energies

In Figure 3.10 we predict the charge distributions of fissioning nuclei ^{222,224,226,228}Th at excitation energies of 35 and 60 MeV. The distributions widen with excitation energies; the explanation is the same as for the U(n, f) case (Chapter 3.2). For the ^{222,224}Th isotopes (Figures 3.10 -a and -b), the central peak recedes and two asymmetric peaks appear, suppressing the symmetric mode. The charge distributions of ^{226,228}Th at higher excitation energies (Figures 3.10 -c and -d) emphasize the asymmetric aspect of the distribution, making the symmetric peak smaller and narrower, and the asymmetric maxima wider and taller.

The average potential energy

$$\langle U(Z_i)\rangle = \frac{\sum_{A_i}\int d\beta_L d\beta_H U(A_i, Z_i, \beta_i, R_m) w(A_i, Z_i, \beta_i, E^*)}{\sum_{A_i}\int d\beta_L d\beta_H w(A_i, Z_i, \beta_i, E^*)}, \tag{3.1}$$

displayed in Figure 3.11, explains the unexpected evolution of the distributions, by presenting asymmetric minimas. These minima are the result of the damping of the surface stiffness coefficient, which leads to a widening of the minima in the deformation plane, and to the enhanced asymmetric emissions.

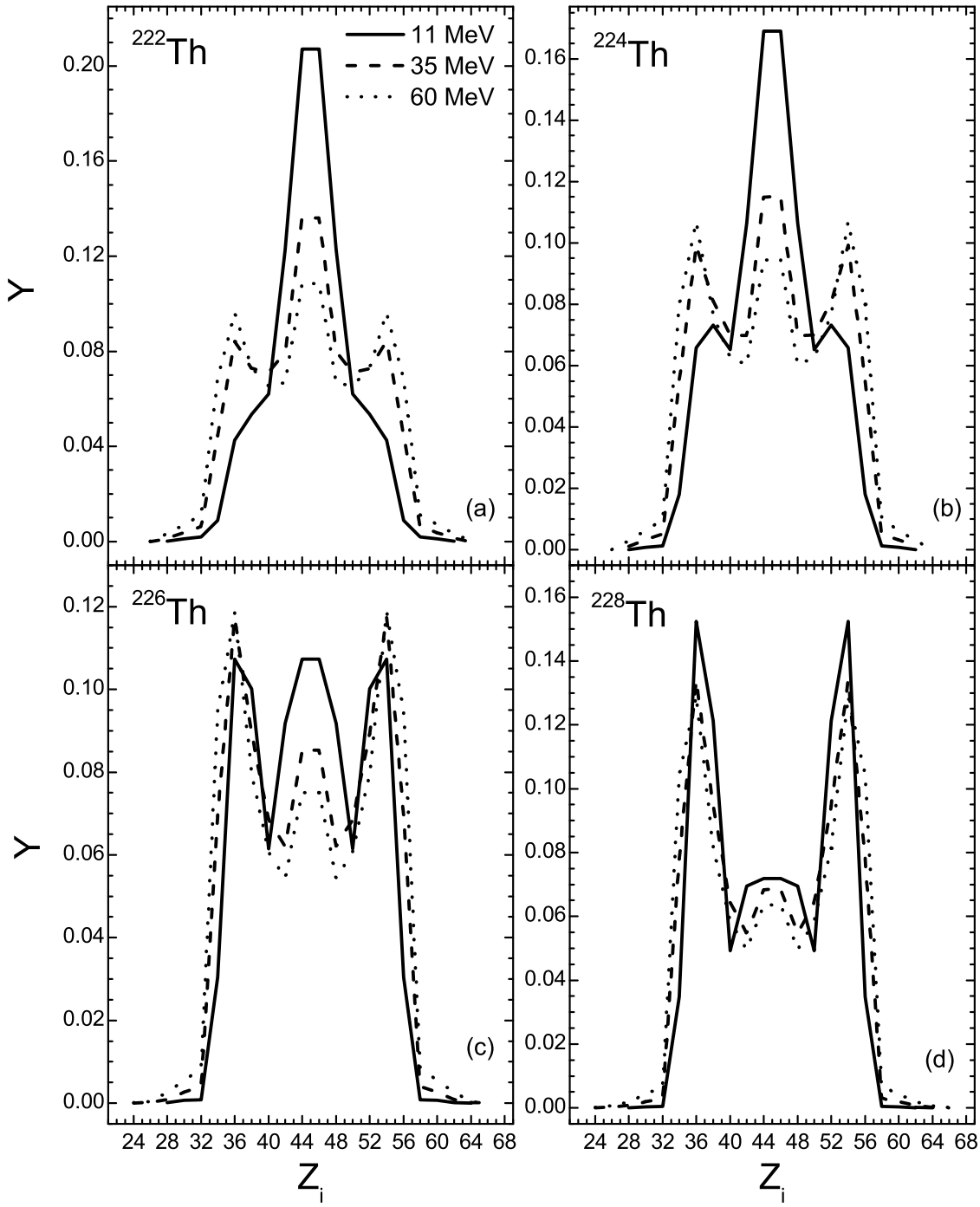

Figure 3.10: The predicted charge distributions for ^{222,224,226,228}Th isotopes at 11, 35, and 60 MeV excitation energies of the initial compound nucleus. The lines connect the calculated yields of even-even fission fragmentations.

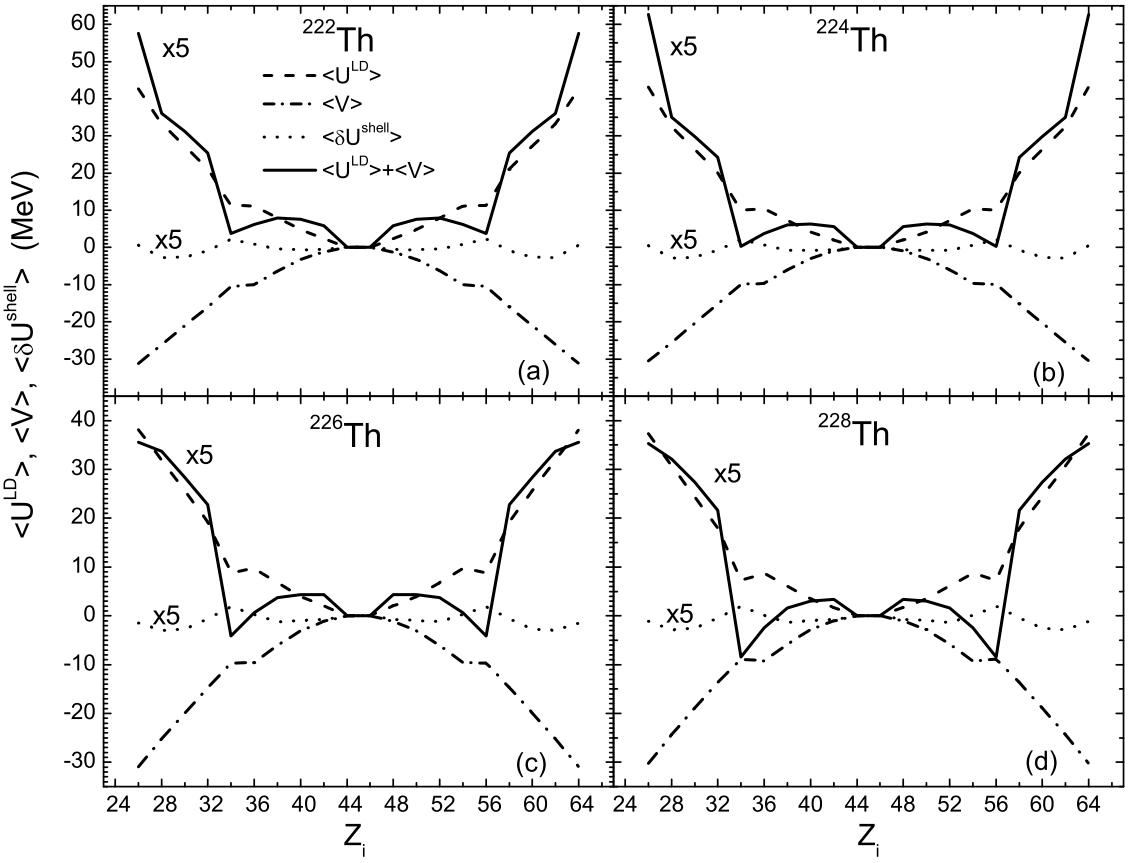

Figure 3.11: The calculated driving potentials $\langle U(Z_i)\rangle$ averaged over the mass number and deformations [Eq. (3.1)] at 60 MeV (solid lines) excitation energy of the initial compound nucleus for indicated fissioning thorium isotopes. The potentials are normalized to the energy $\langle U(Z_L = 44)\rangle = 0$ MeV. The lines connect the points corresponding to the even-even fission fragments.

3.2.2 The fission of N ~ 136 nuclei

It is known from the experimental data that the electromagnetic induced fission of ^{226}Pa shows a three-peaked distribution, and the charge distributions of fissioning $^{224-228}$Pa nuclei present a similar pattern as in the case of Th isotopes. The evolution of the same experimental distributions with increasing neutron number in the case of $^{223-225}$Ac isotopes also display similar features (see Ref. [32], for example). One cannot help but wonder if a similar behavior exists for other elements with neutron number $N \sim 136$. To give an answer to this question we calculated the charge distributions of several even-even Ra isotopes, shown in Figure 3.12. Our model predicts an analogous evolution to that of the Thorium nuclei.

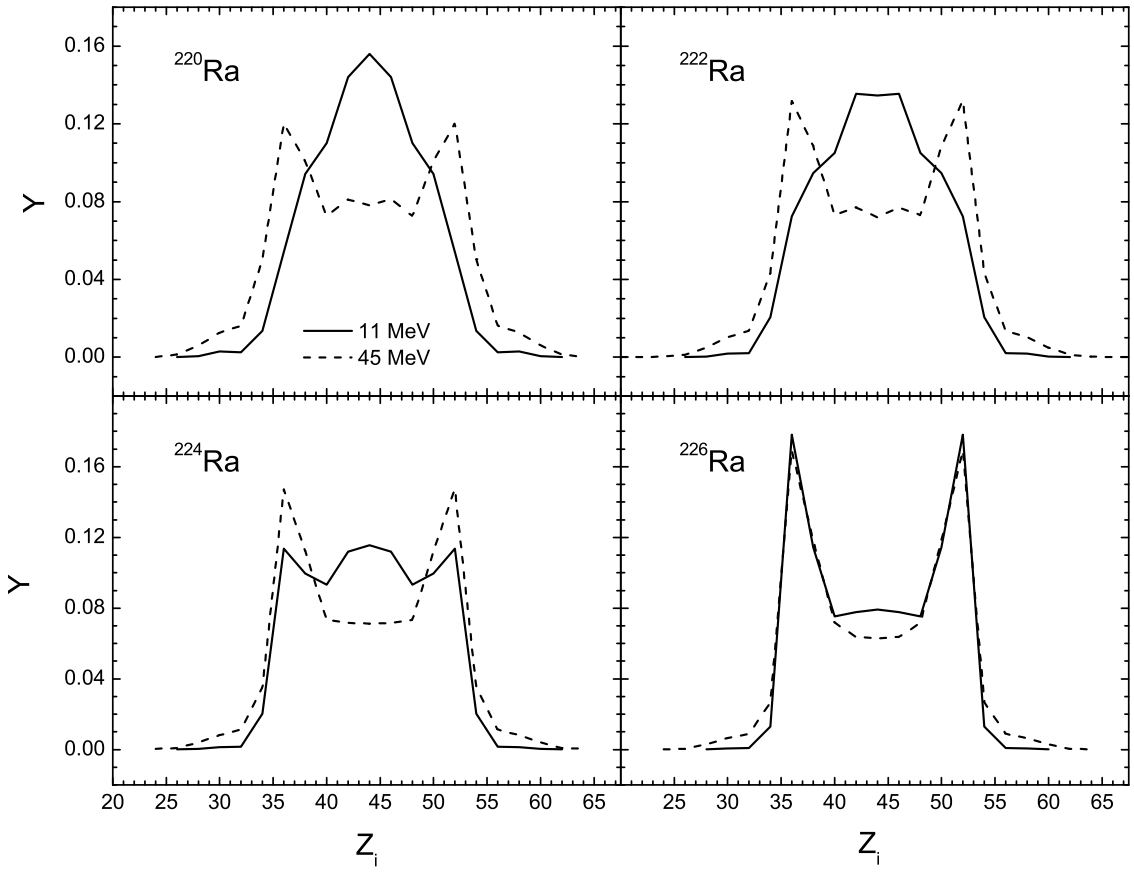

Figure 3.12: Predicted charge distribution for the electromagnetic fission of ^{220,222,224,226}Ra at 11 MeV (solid line) and 45 MeV (dashed line) excitation energies of the initial compound nuclei. The lines connect the calculated points for even-even fission-fragments.

3.3 The Total Kinetic Energy (TKE)

After the system decays and the two fragments become separated in the R coordinate, the interaction energy of the system at the scission point transforms into kinetic energy. The mean total kinetic energy of the system is an important fission characteristic, as it represents most of the released energy of the reaction. For the current study, the TKE distribution represents a mean to check if our calculated potential energy surfaces are realistic.

In Figure 3.13 [22] the TKE dependency on the mass number of the heavy fragment in the case of neutron induced fission of ^{239}Pu is shown. It is worth mentioning the fact that the experimental data represent fragment measurement after the primary neutron emission, and the present calculations are done for the primary fragments, so the theoretical values are a couple of MeV over the experimental values. The pre-neutron TKE distri-

bution was calculated by a Monte-Carlo method in [31]. It was concluded that the neutron emission lowers the TKE values by approximately 7 MeV.

In Figure (3.14) the variation of the average total kinetic energy $< \overline{TKE} >$ (Equation 2.37) with bombarding energy E_n is presented. Qualitatively, the general trend of the evolution is well reproduced, even though there is a systematic $\sim$ 6 MeV overestimation.

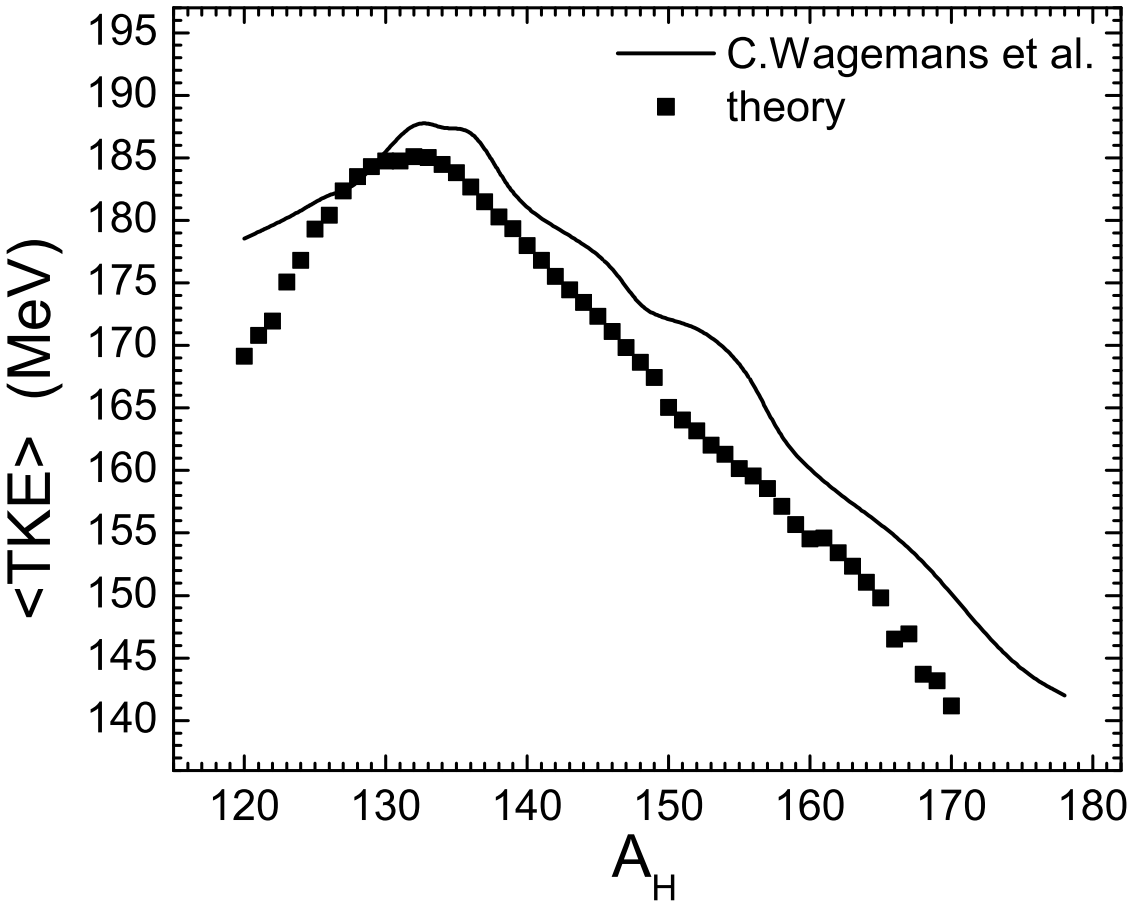

Figure 3.13: The calculated (solid line) fragment mass distribution in the ^{239}Pu(n_{th},f) reaction is compared with the experimental data (symbols) from Ref.[33].

The explanation for the decrease of $< \overline{TKE} >$ with increasing neutron energy, once again relies in the shell damping and surface rigidity "softening" at large excitation energies, which cause the minima in the PES to migrate to more deformed configurations. Still the variations are somewhat modest - 5-6 MeV for a 50 MeV increase of bombarding energy.

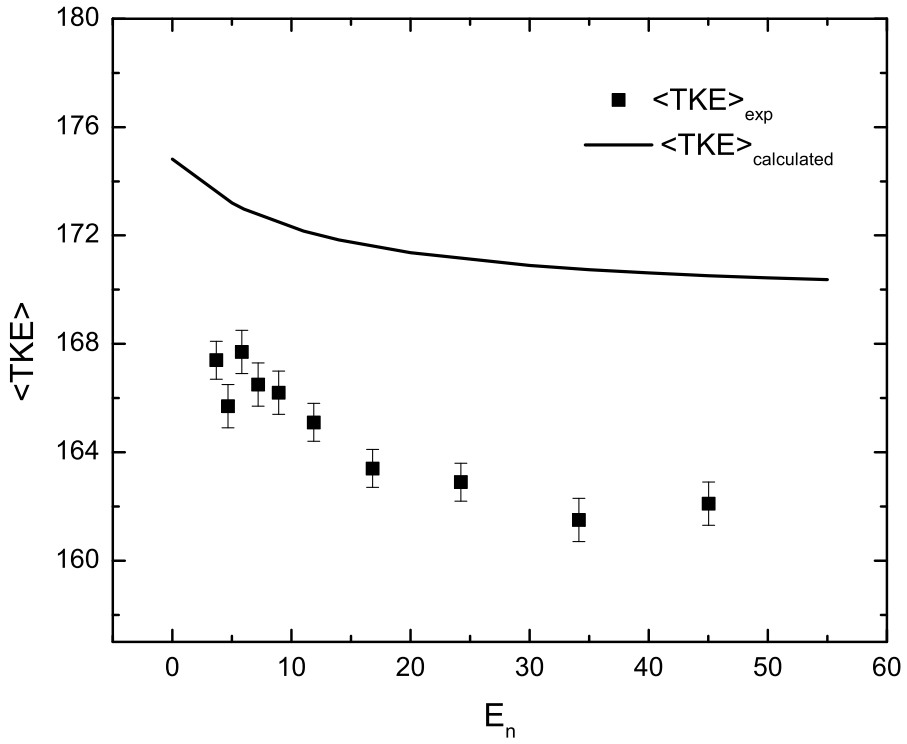

Figure 3.14: Average total kinetic energy calculated for different energies of the incident neutron for the ^{235}U(n, f) reaction. Experimental data taken from [39].

Heavy-ion reactions

4.1 Introduction

In the previous Chapters, the main focus was given to the spontaneous, electromagnetic and neutron induced fission. In all cases the the rotation energy of the system is practically zero. However there is no reason why one can not freely take into account the angular momentum. In Chapter the focus is shifted towards the question "What is the angular momentum of the fission fragments?". Te studies about the spin distributions offer valuable information about the transfer mechanism of the angular momentum from the orbital motion of the system to the intrinsic fission fragment angular momenta, as well as information about the excitation of the collective degrees of motion.

In the classical picture the two nuclei are assumed to be two rigid spheres rotating around a common center (Refs. [41, 40], for example). As the nuclei interact trough long-range repulsive Coulomb forces and short-range attractive nuclear forces, torques are generated upon the two nuclei causing their intrinsic rotation at the expense of relative angular momentum. If the condition of long interaction times is satisfied, the system attains equilibrium which corresponds to rigid rotation, characterized by matching the orbital and intrinsic angular velocities. The angular momenta of one of the nuclei after break-up is given by:

$$< I_i >= \frac{\Im_i}{\Im_1 + \Im_2 + \mu R_m^2} J, \tag{4.1}$$

are the angular momentum and moment of inertia of the fragment i, μR_m^2 is the relative moment of inertia and J is the angular momentum of the system.

In an experiment, the measurement of γ-ray multiplicities and alignment of the fragment spins provides insight to the process of angular momentum transfer. An often used relationship between γ-ray multiplicity M_γ and

angular momentum I is given in literature as:

$$< I^T_{Z,A} >= 2[M_\gamma(Z,A) - a_\gamma], \tag{4.2}$$

where a_γ is a constant between 1 and 6 and is the number of statistical transitions that can be inferred from the $\gamma-$spectrum and that are weakly related to the collective spin.

4.2 Transfer of orbital angular momentum to the fission fragments. The orbital component

The centrifugal potential can be written as:

$$V_R(R,Z,A,\beta_1,\beta_2) = \frac{\hbar^2 J(J+1)}{2\Im(R,A,\beta_1,\beta_2)} + E_{bm}, \tag{4.3}$$

where the moment of inertia of the DNS is $\Im_{DNS}(A,R,\beta_H,\beta_L) = \Im_H + \Im_L + \mu R^2$ and the moments of inertia of the nuclei $i = H, L$ are calculated as [28]:

$$\begin{aligned}
\Im_i &= \frac{1}{5} m_0 r_0^2 A^{\frac{5}{3}} (a_i^2 + b_i^2), \\
a_i &= \left(1 - \frac{\beta_i^2}{4\pi}\right)\left(1 + \sqrt{\frac{5}{4\pi}}\beta_i\right), \\
b_i &= \left(1 - \frac{\beta_i^2}{4\pi}\right)\left(1 - \sqrt{\frac{5}{16\pi}}\beta_i\right).
\end{aligned} \tag{4.4}$$

Taking into account the angular momentum, the quasifission barrier becomes:

$$B_R^{qf}(Z,A,J) = V(R_b,Z,A,\beta_1,\beta_2,J) - V(R_m,Z,A,\beta_1,\beta_2,J). \tag{4.5}$$

In the first stage of heavy ion collision, if the incoming nucleus has enough kinetic energy to overcome the Coulomb barrier, it is captured by the target nucleus. The kinetic energy of the projectile $E_{c.m.}$ and the angular momentum J of the relative motion is transformed into excitation energy and angular momentum of the DNS. The partial capture cross section which characterizes the formation of the initial DNS is:

$$\sigma_{cap}(E_{c.m.},J) = \pi \lambda\!\!\!^{-2}(2J+1) P_{cap}(E_{c.m.},J). \tag{4.6}$$

In the above equation, $\lambda\!\!\!^{-2} = \hbar^2/2\mu E_{c.m.}$ is the reduced de Broglie wavelength, and the capture probability $P_{cap}(E_{c.m.}, J)$ is given by the Hill-Wheeler formula. [27]. The total capture cross section is given by:

$$\sigma_{cap}(E_{c.m.}) = \sum_{J=0}^{J_{max}} \sigma_{cap}(E_{c.m.}, J). \tag{4.7}$$

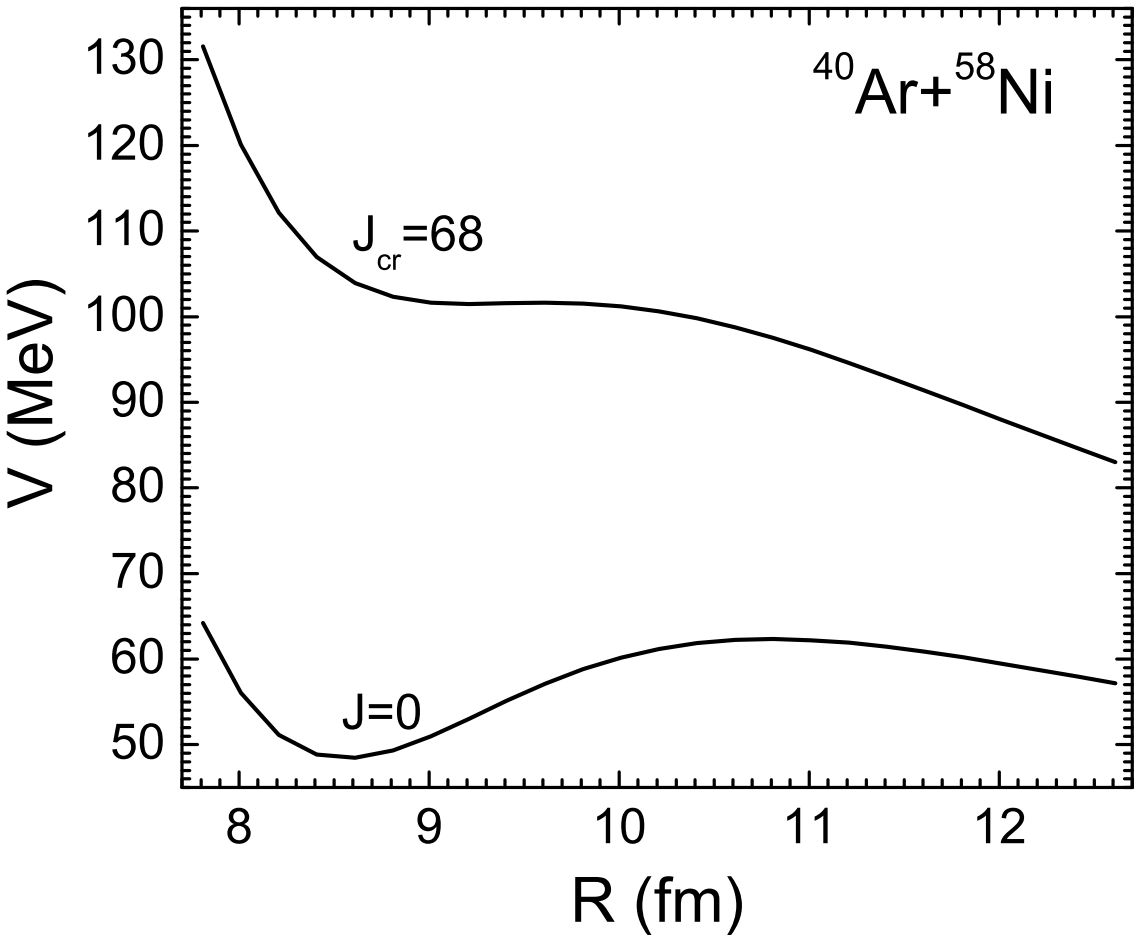

Figure 4.1: The nucleus-nucleus interaction potential for the ^{40}Ar + ^{58}Ni reaction at $J = 0$ and $J = J_{cr} = 68$.

The maximum value for the angular momentum J_{max} is limited by the value of the critical (the value of J for which the potential pocket disappears) or of the kinematic angular momentum
$J_{kin} = \sqrt{2\mu[E_{c.m.} - V(R_b, Z_i, A_i, J = 0)]}R_b/\hbar$, depending on which one is smaller $J_{max} = \min[J_{kin}, J_{cr}]$.

The evolution of the system in mass and charge coordinate is completely

determined by the driving potential, defined as [5]:

$$U = V(R, Z, A, J, \beta_1, \beta_2) + B_1 + B_2 - B_{CN} - E^{rot}_{CN}(J), \tag{4.8}$$

where B_{CN} și $E^{rot}_{CN}(J) = \hbar^2 l(l+1)/2\Im_{CN}$ are the mass excess (taken from ref.[47, 48]) and rotational energy of the CN, respectively, and $B_{1,2}$ are the mass excesses of the fragments.

Taking into account the angular momentum, the excitation energy E^* of the CN is calculated with the formula:

$$E^*_{CN}(J) = E_{c.m.} + B_1 + B_2 - B_{CN} - E^{rot}_{CN}(J), \tag{4.9}$$

where $B_1 + B_2 - B_{CN}$ is the reaction Q value. The rotational energy $E^{rot}_{CN}(J)$ is not available for internal excitation. The excitation energy of the scission configuration can now be written as: $E^*_{DNS} = E^*_{CN}(J) - U(R_m, Z, A, J)$.

The probability of the DNS formation, decay and total emission probabilities are given by Equations (2.26, 2.28) and (2.29). For a nucleus with a given charge Z and mass number A, the production cross section is calculated as:

$$\begin{aligned}\sigma_{Z,A}(E_{c.m.}) &= \sum_{J=0}^{J_{max}} \sigma_{Z,A}(E_{c.m.}, J) = \\ &= \sum_{J=0}^{J_{max}} \sigma_{cap}(E_{c.m.}, J) W_{Z,A}(E^*_{CN}, J).\end{aligned} \tag{4.10}$$

Replacing I_0 in Equation (4.1) with the average value $< J >_{Z_i,A_i}$ we obtain the angular momentum of the fragment (Z_i, A_i):

$$I_{Z_i,A_i} = \frac{\Im_i}{\Im_1 + \Im_2 + \mu R_m^2} \frac{\sum_{J=0}^{J_{max}} J\sigma_{Z_i,A_i}(E_{c.m.}, J)}{\sum_{J=0}^{J_{max}} \sigma_{Z_i,A_i}(E_{c.m.}, J)}. \tag{4.11}$$

The angular momenta as a function of the mass or charge numbers I_{Z_i} and I_{A_i} are obtained by summing over the relevant numbers.

4.2.1 The angular momentum bearing modes

The orbital motion of the system is not the only source of intrinsic spin of the fragments. Collective angular oscillations are also generated by thermal excitation of the pre-scission DNS. These modes (bending, wriggling,

tilting and twisting) contribute to the angular momenta and rotational energy of the fission fragments. These degrees of freedom can be easily identified. Let us fix a reference frame with the y axis coincident with the line of centers and the x and z axes perpendicular to it. The two bending modes correspond to a rotation of one fragment parallel to the x or z axis associated with an opposite rotation of the other fragment. The twisting modes correspond to a rotation of one fragment about the y axis associated with an opposite rotation of the other fragment. The two wriggling modes are rotations of both fragments parallel to the x or z axis compensated by a counter-rotation of the system as a whole about the same axis. Finally the tilting mode describes the inclination angle of the total angular momentum with respect to the y axis. In general, since these collective modes are not exactly normal but are weakly coupled to the intrinsic modes, they can be thermally excited.

Taking into account the angular momentum bearing modes, the average angular momentum of the fragment can be written as:

$$< I_{Z,A} >= \frac{\sum_{J=0}^{J_{max}} I_{Z,A}^{T}(J)\sigma_{Z,A}(E_{c.m.},J)}{\sum_{J=0}^{J_{max}} \sigma_{Z,A}(E_{c.m.},J)}, \tag{4.12}$$

where:

$$\begin{aligned} I_{Z,A}^{T}(J) &= I_{Z,A}^{Rigid}(J) + I_{Z,A}^{Bearing}(J) \\ &= I_{Z,A}^{Rigid}(J) + I_{Z,A}^{Tw}(J) + I_{Z,A}^{Ti}(J) + I_{Z,A}^{B}(J) + I_{Z,A}^{W}(J) \end{aligned} \tag{4.13}$$

I_i^W. is the sum of the pure orbital I_i^{Rigid}, twisting I_i^{Tw}, tilting $I_{Z,A}^{Ti}$, bending I_i^B, and wriggling I_i^W spin components of the fragment.

In Ref.[52] the wriggling mode, consisting of the rotation of both fragments in the same direction (the light nucleus carries the bulk of the spin) and the rotation of the whole system in the opposite direction is also described. Although this motion is possible in the classical description, quantum mechanical calculations show that the energy needed to activate this mode is much higher than the energy needed for the twisting, tilting and bending modes. In the fact, it is energetically costly to impart spin to the light fragment. In comparison, for the bending and tilting modes, the heavy fragment bears most of spin in the asymmetric DNS and for the twisting mode, both fragments carry equal spins for any DNS.

4.2.2 Widths

The standard deviation of the fragment $(Z_i, A_i), i = 1, 2$ is:

$$\sigma_{Z_i,A_i} = \frac{\Im_i}{\Im_1 + \Im_2 + \mu R_m^2} \sqrt{< J^2 >_{Z_i,A_i} - < J >^2_{Z_i,A_i}}. \tag{4.14}$$

The total fluctuation that originates from orbital motion is then:

$$\sigma_{Orbital} = \sqrt{\sigma^2_{Z_1,A_1} + \sigma^2_{Z_2,A_2}} \tag{4.15}$$

The large dispersion in the spin distribution of the fragments can not be explained only by the contribution from the width of the orbital angular momentum distribution. As was shown in ref.[52] the contribution from the bending and twisting modes must be taken into account.

The expressions for the variances arising from bending and twisting modes are [52]:

$$\sigma^2_{Bending} = (|a_{1B}| + a_{2B})^2 \tau, \tag{4.16}$$

$$\sigma^2_{iTwisting} = a^2_{iTw} \left(1 - \frac{2}{\pi}\right) \tau. \tag{4.17}$$

In the above equations τ is the average temperature of the DNS:

$$\tau = \frac{\sum_{J=0}^{J_{max}} T_{DNS}(J) \sigma_{Z,A}(E_{c.m.})}{\sum_{J=0}^{J_{max}} \sigma_{Z,A}(E_{c.m.})} \tag{4.18}$$

The spin distribution of the fission fragments

As a first example we show the calculated results for the 166 MeV ^{20}Ne+^{63}Cu reaction leading to the CN ^{83}Y($E^*_{CN}(J = 0) = 125MeV$). The maximum angular momentum is $J_{max} = 51$.

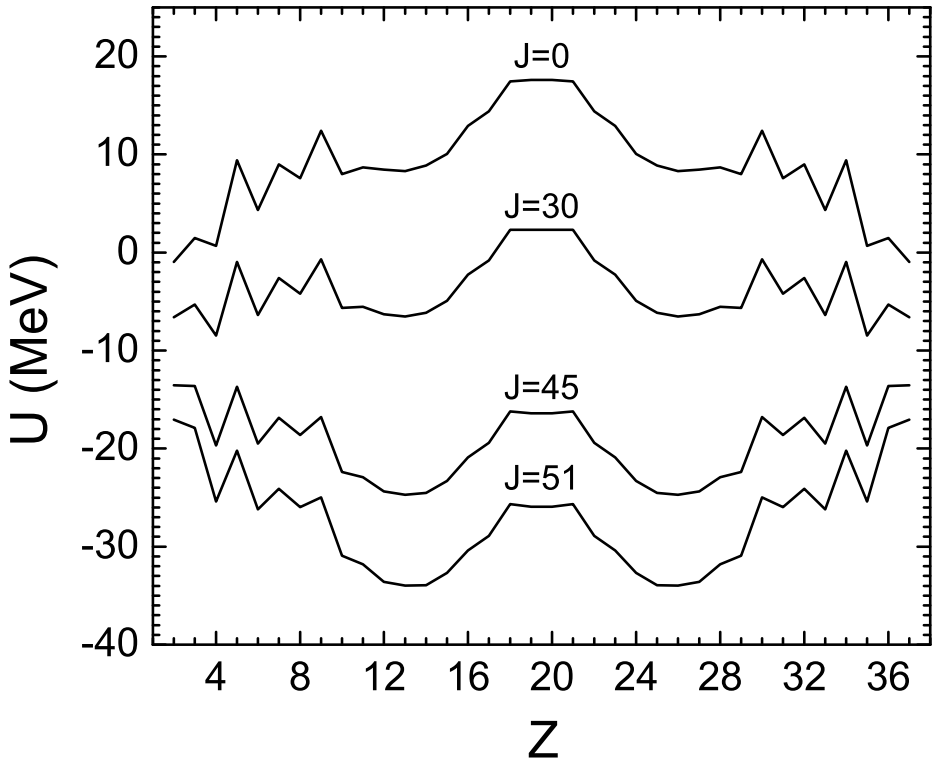

Figure 5.1: Driving potential for the ^{20}Ne+^{63}Cu system at different angular momenta.

In Figure 5.1 the driving potential of the system ^{20}Ne+^{63}Cu is presented at different values of the angular momentum J, normalized to the value of the rotating compound nucleus. One can notice that above a certain value of J, U becomes negative, i.e. from an energetic point of view, the DNS configuration is more favourable than the CN one. This indicates that the

complete fusion is energetically forbiden, and the quasi-fission is the main reaction mechanism.

With the help of Equation (4.2) and (4.12) one can calculate the average γ-ray multiplicity from the sum of the spins $< I^T_{Z_1} > + < I^T_{Z_2} >$ of the two fragments (Figure 5.2)..

By using Equations (4.14-4.17) the widths of the spin distribution can be calculated (Figure 5.3). By adding the contribution from the orbital motion to the contributions from the angular momentum bearing modes, the total width remains approximately constant, in agreement with experimental data.

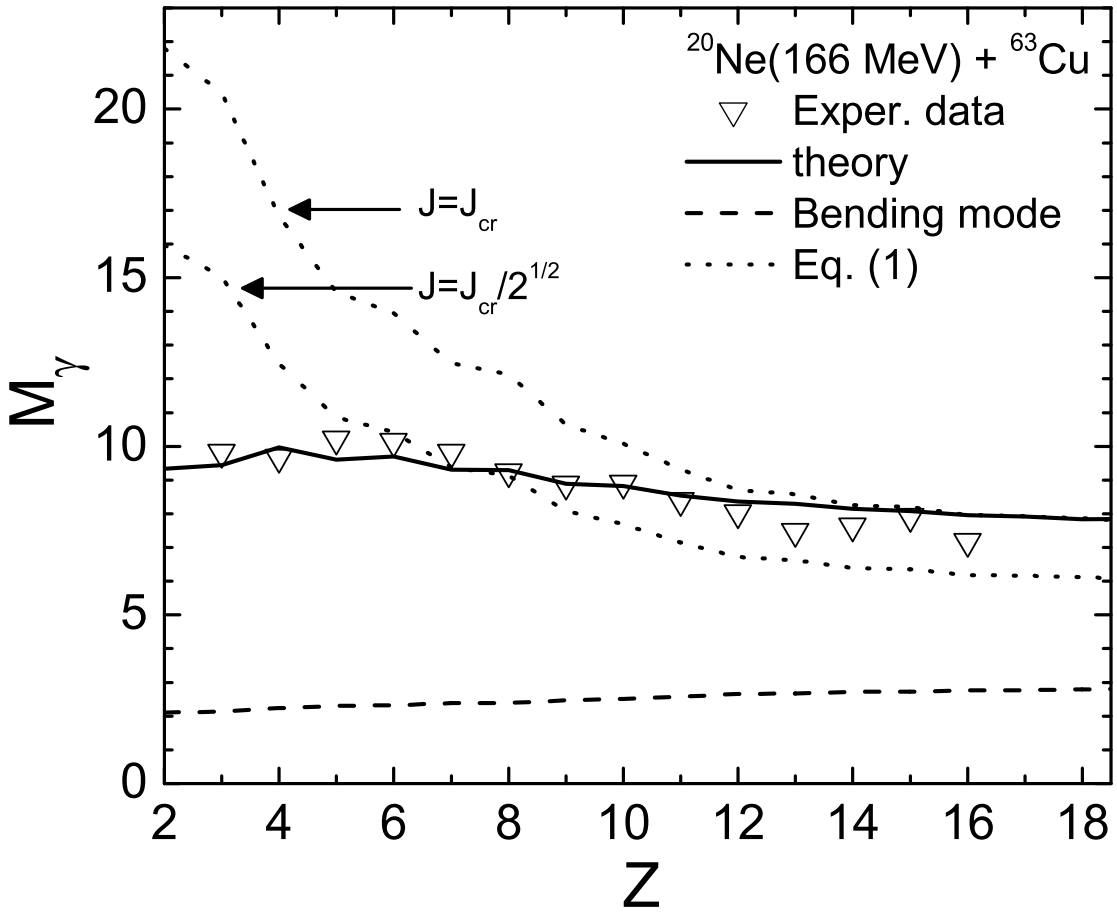

Figure 5.2: The calculated (solid line) gamma-ray multiplicities (a_γ = 0) deduced from the calculated sum of the fragment spins as a function of charge number of one of the fragments in the ^{20}Ne(166 MeV)+^{63}Cu reaction. The contribution from the bending mode is shown by dashed line. The results of calculations with Eq. (4.1) and $J = J_{cr}, J_{cr}/\sqrt{2}$ are indicated by dotted lines The experimental data (open triangles) are from Ref. [51].

To emphasize the role of our model, the angular momenta of the two

fragments is calculated with Equation (4.1) and is shown (Figure 5.2) for two values of I_0, $I_0 = J_{cr}$ and $I_0 = J_{cr}/\sqrt{2}$. While this simple formula can describe the experimental data for symmetric fragmentation of the CN, it fails to give an accurate result as one goes to large asymmetries.

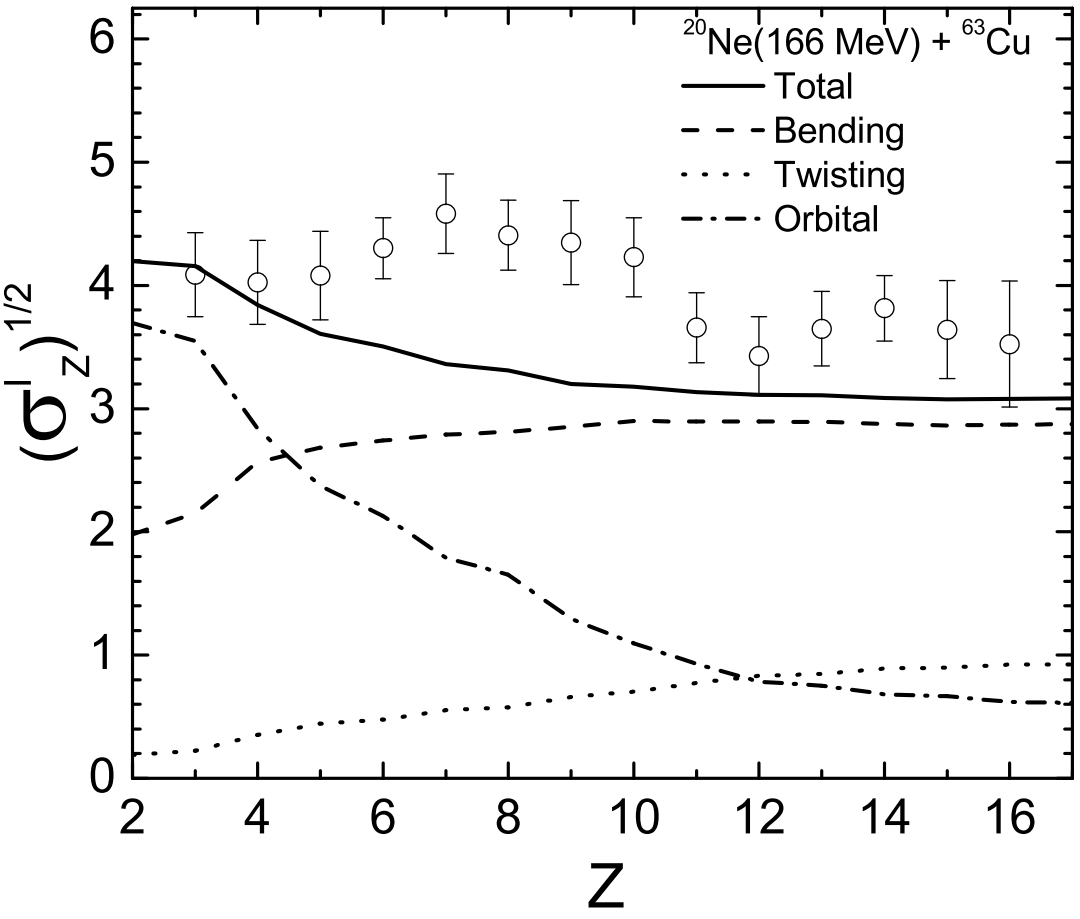

Figure 5.3: The calculated root of the total widths (solid line) of the spin distributions versus the charge number of the light fragment in the ^{20}Ne(166 MeV) + ^{63}Cu reaction. The contributions from the orbital motion (dash-dotted line), bending (dashed line), twisting (dotted line) modes are shown. The experimental data (open circles) are from Ref. [51].

5.1 Role of formation and decay probabilities. Comparison with other models

In Figure 5.4 the average γ-ray multiplicities are calculated for the 175 MeV ^{20}Ne+Ag reaction which leads to the CN ^{127}La ($E^*_{CN}(J = 0) = 128MeV$). The value of the maximum angular momentum is set to $J_{cr} = 63$. To emphasize the role of the formation and decay probabilities even

further in Equation (4.11) we show for comparison the case where $W_{Z,A}(E_{c.m.}, J) = 1$ for all nuclei, i.e. all fragmentations are equally possible.

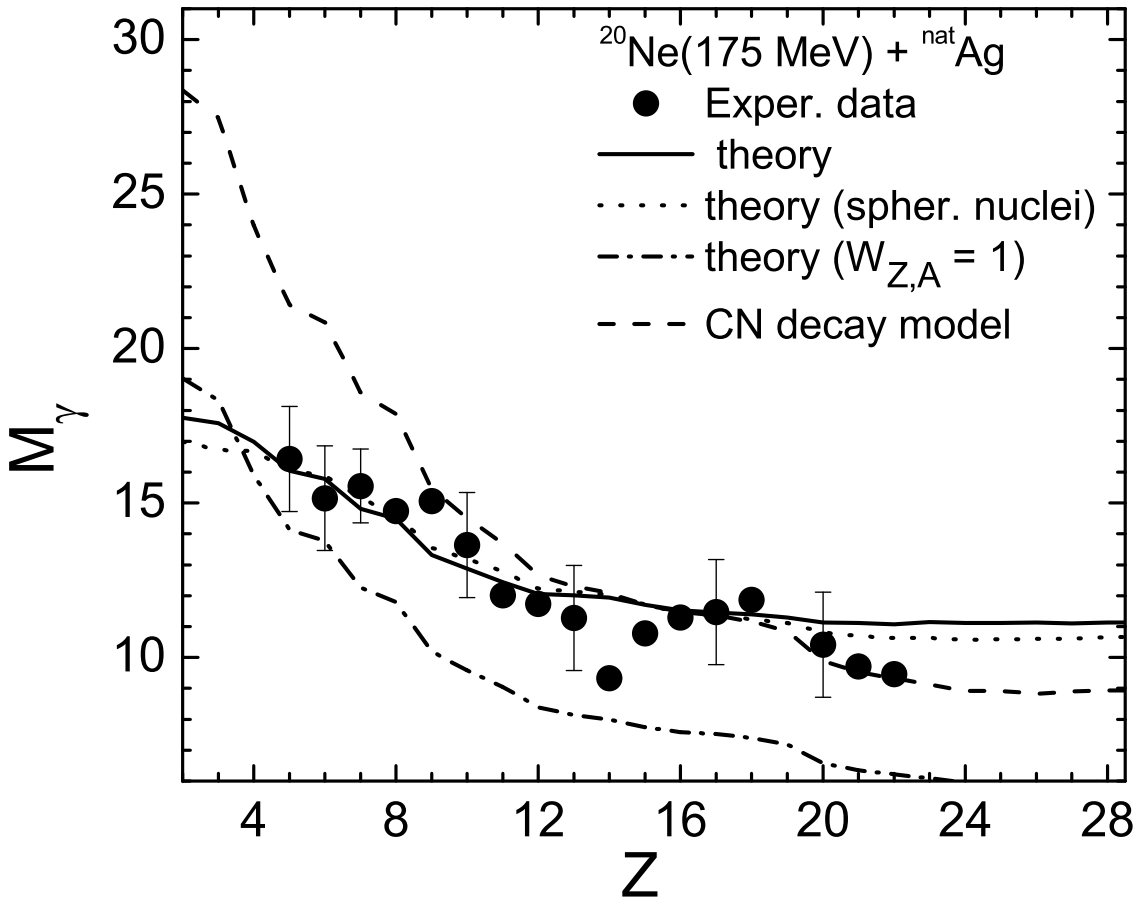

Figure 5.4: The calculated sum of the average fragment spins with (solid line) and without (dotted line) considering the fragment deformations in the ^{20}Ne(175 MeV)+^{nat}Ag reaction. The results calculated with Eq. (**??**) (dash-dotted line) and with the CN decay model of Ref. [50] (dashed line) are also plotted. The conversion from the gamma-ray multiplicities to the fragment spins is performed with Eq. (4.2) and $a_\gamma = 1$.

For comparison we also present the results of the calculations without taking into account the effect of deformations (dotted line). One can see that the dependence on deformations is rather weak. Also, the results of using a CN decay model is also used[50].

5.2 Role of the entrance channel

5.2.1 Role of the center of mass energy

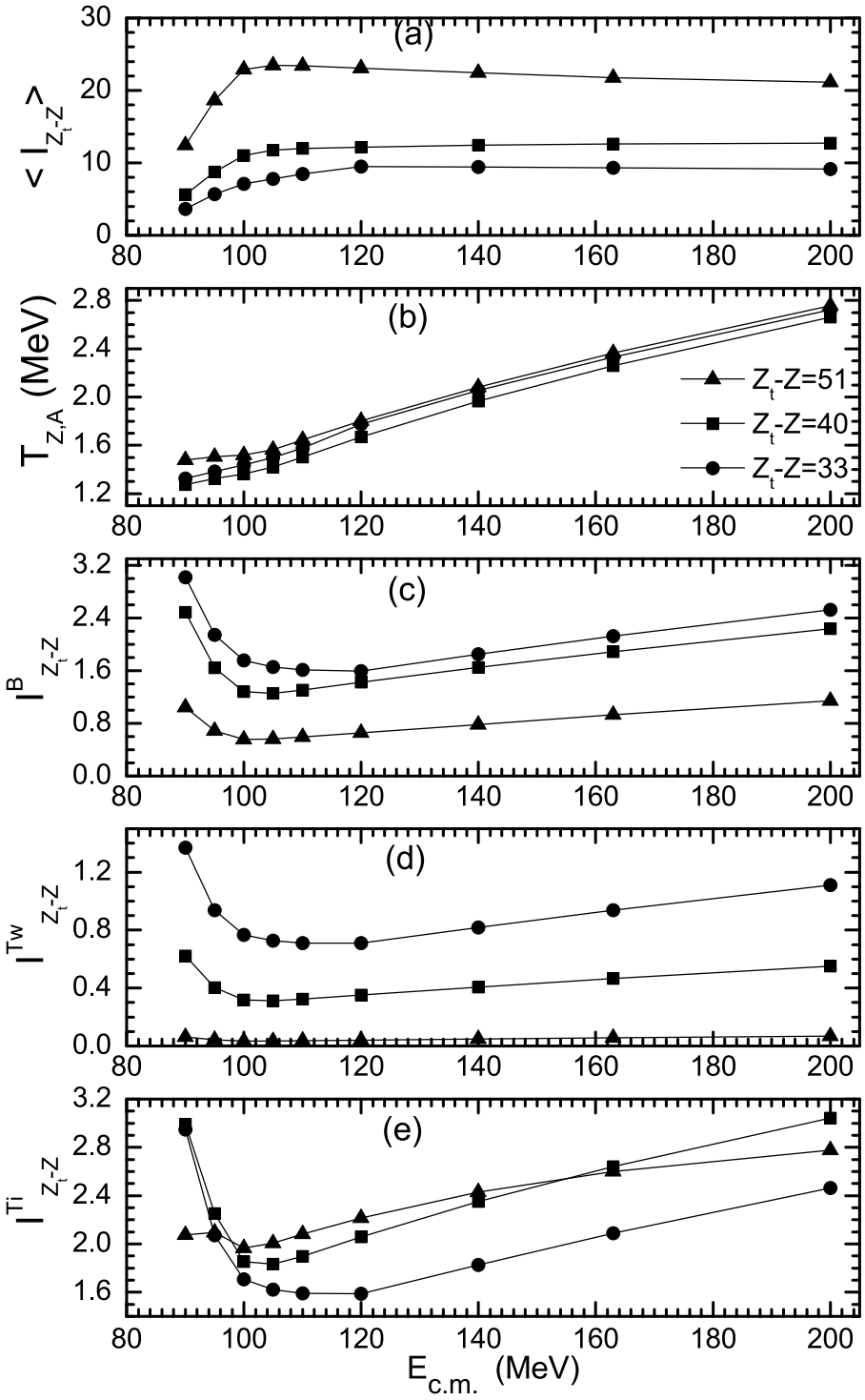

Figure 5.5: (a) The average angular momentum of the fission fragment due to the orbital motion and (b)average temperature of the DNS. The panels (c), (d) and (e) are the spin components arising from the excitation of the bending, twisting and tilting modes, respectively, of the fragments with $Z_t - Z$ =33 (circles), 40 (squares), and 51 (triangles) as a function of the center of mass energy in the ^{40}Ar+^{89}Y reaction.

An important parameter which governs the nucleus-nucleus collisions is the kinetic energy of the incident projectile, which determines key aspects of the reaction, such as: the fusion cross section, the angular momentum injected into the system, etc..

In Figure 5.5 the evolution of the different components of the spin are displayed as a function of the bombarding energy in the reaction ^{40}Ar+^{89}Y. The most important aspect is the predicted saturation of the orbital component of the angular momentum above a certain value of the kinetic energy.

5.2.2 Role of mass asymmetry in the entrance channel

To investigate the influence of the mass asymmetry in the entrance channel on spin distribution we chose the reactions [49] ^{48}Ca+^{86}Kr (5.5 MeV/nucleon, J_{max} = 88) and ^{12}C+^{122}Sn (12 MeV/nucleon, J_{max} = 47) [49]. Both reactions lead to the same CN, ^{134}Ba, with the same excitation energy $E^*_{CN}(J = 0)$ = 130 MeV. For these reactions J_0 = 70, which means that for the asymmetric ^{12}C+^{122}Sn system the fragments are produced by CN decay. For the ^{48}Ca+^{86}Kr system, when $J > J_0$ the symmetric DNS configuration becomes energetically favorable.

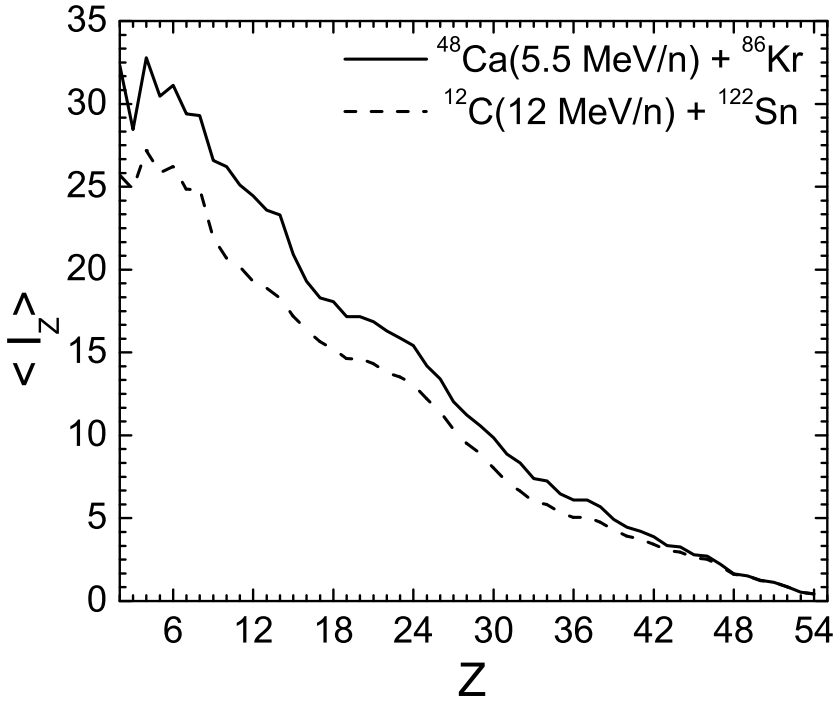

Figure 5.6: Average angular momentum of the heavy fragment as a function of the atomic number of the light fragment for the 5.5 MeV ^{48}Ca+^{86}Kr (solid line) and 12 MeV ^{12}C+^{122}Sn (dashed line) reactions.

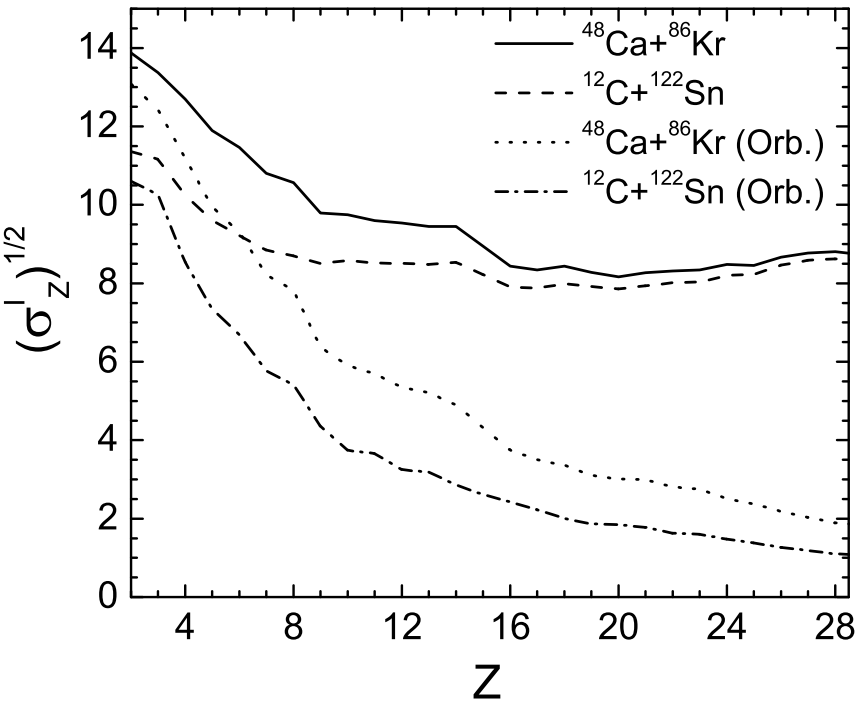

Figure 5.7: Widths of the spin distribution for the same reactions as Figure (5.6).

Conclusions

In the current work the DNS model was employed for the description of the fission process. The theoretical results were compared with the experimental data, and excellent results were obtained. The main ingredient of our model is the calculation of the potential energy surfaces (PES). One of the contributions brought to the model is the restriction of the number of the allowed configurations by limiting the minimum value of the quasi-fission barrier. This simple restriction excludes the strongly deformed and unrealistic configurations at the scission point. Also, this restriction "simulates" some dynamical effects, while still retaining all of the features of the statistical model.

Another important contribution is the inclusion of temperature dependent terms in the total energy, as well as the introduction of a temperature dependent surface stiffness coefficient. Together with the well-known excitation dependence of the shell corrections, these improvements allow the model to describe a large collection of experimental data, such as: the mass-, charge-, isotopic-, TKE-,and spin-distributions, and neutron multiplicities. In the case of the reactions presented, the evolution of these observables with increasing excitation energy (up to 60 MeV) was studied. The changes observed are shown to be related to the energy-dependent structures in the PES.

In the case of the charge (mass) distributions, the main result is the conservation of the asymmetric shapes in the fission of U and Pu isotopes, in agreement with the experimental data. Furthermore, the model predicts strong asymmetric modes in the case of fissioning thorium isotopes at large excitation energies. Charge distributions with equal asymmetric and symmetric components were predicted for several isotones.

When it comes to heavy-ion collisions, the formalism developed in the DNS model allows for a correlation between the fission-fragment angular momenta and the other fission observables such as the mass and charge of the fission fragments, production cross-sections, and, more importantly, to the entrance channel. The comparisons with the experimental data show an excellent agreement for both the average values as well as for the widths

of the distributions. The collective angular momentum bearing modes are incorporated into our model in a natural way. One of the main results is the saturation of the orbital component of the fission fragment's spin. The distinction between the compound nucleus decay and the cvasifission channel is given, based on the shape of the spin distributions. The saturation of the orbital component of the fragment's intrinsic spin is predicted.

Bibliography

[1] K.H. Schmidt and B. Jurado *General Laws of Quantum and Statistical Mechanics Governing Fission*, in *Nuclear Physics: Present and Future*, Ed. by W. Greiner (pp. 121-129). (Springer International Publishing, 2015).

[2] U. Mosel, H. W. Schmitt, *Potential energy energy surfaces for heavy nuclei in the two-center shell model*, Nucl. Phys. A **165**, 73 (1971)

[3] A.V. Andreev, *Theory of binary and ternary fission based on the scission-point model*, (Unpublished doctoral thesis), Justus-Liebig-University, Gissen, Germany (2006)

[4] A. Bohr and B. Mottelson, *Nuclear Structure* (W. A. Benjamin, New York, Ams- terdam, 1974).

[5] G. G. Adamian *et al.*, Int. J. Mod. Phys. E **5**, 191 (1996).

[6] C. Y. Wong, Phys. Rev. Lett. bf 31, 766 (1973).

[7] M. Ivascu, D.N. Poenaru, *Energia de deformare si izomeria formei nucleelor*, (Ed.Academiei Republicii Socialiste Romania, Bucuresti 1981)

[8] A.V. Andreev, G.G. Adamian, N.V. Antonenko, S.P. Ivanova,

[9] W. Greiner, J. Y. Park, and W. Scheid, *Nuclear Molecules* , (World Scientific, Singapore, 1995).

[10] S. Raman, C. W. Nestor, and P. Tikkanen, At. Data Nucl. Data Tables **78**, 1 (2001).

[11] P. Möller and R. Nix, At. Data Nucl. Data Tables **39**, 213 (1988)

[12] P. Möller and R. Nix, Nucl. Phys. A **361**, 117 (1980); LANL Preprint LA-UR-86-3983 1986.

[13] W. Greiner, J. Maruhn, *Nuclear Models*, (Springer-Verlag Berlin Heidelberg, Germany, 1996)

[14] R. Berginger, W.J. Knox, Phys. Rev., *121*, 192 (1961)

[15] V.M. Strutinsky, Yad. Fiz., *3*,614 (1966)

[16] V.M. Strutinsky, Nucl. Phys. A, *95*, 420 (1967)

[17] V.M. Strutinsky, Yad. Fiz., *122*, 1 (1968)

[18] M. Brack, *et.al.*, *Funny hills: The shell-correction approach to nuclear shell effects and it's application to the fission process*, Rev. Mod. Phys.,**44**, 2 (1972)

[19] J. Maruhn and W. Greiner, Z. Physik **251**, 431 (1972)

[20] A. V. Ignatyuk, *Statistical Properties of Excited Atomic Nuclei*, (Energoatomizdat, Moscow, 1983)

[21] **H. Paşca**, A.V. Andreev, G.G. Adamian, N.V. Antonenko, and Y. Kim, Phys. Rev. C **93**, 054602 (2016); H. Paşca, EPJ Web of Conferences **107** 07003 (2016), DOI: 10.1051/epjconf/201610707003.

[22] **H. Paşca**, A.V. Andreev, G.G. Adamian, and N.V. Antonenko, Phys. Rev. C **94**, 064614 (2016)

[23] **H. Paşca**, A.V. Andreev, G.G. Adamian, and N.V. Antonenko, Phys. Lett. B **760**, 800 (2016).

[24] **H. Paşca**, A.V. Andreev, G.G. Adamian, and N.V. Antonenko, Eur. Phys. J. A **52**, 369 (2016)

[25] G. Sauer, H. Chandra, and U. Mosel, Nucl. Phys. **A264**, 221 (1976).

[26] B.D. Wilkins, E. Steinberg, R. Chasman, Phys. Rev. C **14**, 1832 (1976)

[27] Sh.A. Kalandarov, G.G. Adamian, N.V. Antonenko, and W. Scheid, Phys. Rev. C **82**, 044603 (2010);

[28] Sh.A. Kalandarov, G.G. Adamian, N.V. Antonenko, and W. Scheid,Phys. Rev. C **83**, 054611 (2011);

[29] Sh.A. Kalandarov, G.G. Adamian, N.V. Antonenko, W. Scheid, and J.P. Wieleczko, Phys. Rev. C **84**, 064601 (2011)

Jolos, Phys. Part. Nuclei 25, 583 (1994);

Antonenko, R. V. Jolos, and A. K. Nasirov, Nucl. Phys. A 551, 321 (1993)

[30] A.J. Cole, *Statistical models for nuclear decay: from evaporation to vaporization*, (Institute of Physics Publishing, Bristol, UK, 2000)

[31] W. Lang, H. G. Clerc, H. Wohlfarth, H. Schrader, and K. H. Schmidt, Nucl. Phys. A **345**, 34 (1980)

[32] K.-H. Schmidt *et al.*, Nucl. Phys. A **665**, 221 (2000).

[33] C. Wagemans, E. Allaert, A. Deruytter, R. Barthelemy, and P. Schillebeeckx, Phys. Rev. C **30**, 218 (1984).

[34] U. Brosa, S. Grossmann, and A. Müller, Phys. Rep. **197**, 167 (1990).

[35] A.N. Andreyev, M. Huyse, and P. Van Duppen, Rev. Mod. Phys. **85**, 1541 (2013).

[36] A.N. Andreyev *et al.*, Phys. Rev. Lett. **105**, 252502 (2010).

Nucl. Phys. **A462**, 85 (1987); F.-J. Hambsch, H.-H. Knitter, and C. Budtz-Jorgensen, Nucl. Phys. **A491**, 56 (1989).

[37] I.V. Ryzhov *et. al.*, Phys. Rev. C **83**, 054603 (2011).

[38] J. Benlliure *et al.*, Nucl. Phys. **A628**, 458 (1998).

[39] R. Yanez, L. Yao, J. King, and W. Loveland, Phys. Rev. C **89**, 051604(R) (2014).

[40] L.G. Moretto, R.P. Schmitt, Phys. Rev. C 21 (1980) p. 204

[41] A. Gobbi, W. Norenberg, *Heavy Ion Collisions* vol. II (North-Holland, 1980), Ch.3, p.226-230

[42] V.V. Volkov, Izv. AN SSSR ser. fiz. **50**, 1879 (1986);

[43] G.G. Adamian, N.V. Antonenko, and W. Scheid, Nucl. Phys. **A618**, 176 (1997);

[44] G.G. Adamian, N.V. Antonenko, W. Scheid, and V.V. Volkov, Nucl. Phys. **A627**, 361 (1997);

[45] G.G. Adamian, N.V. Antonenko, W. Scheid, and V.V. Volkov, Nucl. Phys. **A633**, 409 (1998);

[46] G.G. Adamian, N.V. Antonenko, and W. Scheid, Phys. Rev. C **68**, 034601 (2003).

[47] G. Audi, A. M. Wapstra, and C. Thibault, Nucl. Phys. A 729,

[48] P. Möller et al., At. Data Nucl. Data Tables 59, 185 (1995).

[49] Sh. A. Kalandarov, G.G. Adamian, N.V. Antonenko, W. Scheid, P. Wieleczko, Phys. Rev. C 00, 004600 (2011)

[50] L.G. Moretto, G.F. Peaslee, G.J. Wozniak, Nucl.Phys. A502, 453c-472c (1989)

[51] R.A. Dayaras, R.G. Stokstad, D.C. Hensley, M.L. Halbert, D.G. Sarantites, L. Westberg, J.H. Barker, Phys.Rev. C22, 1485 (1980)

[52] R.P.Schmitt, A.J.Pacheco, Nucl.Phys. A379, 313 (1982)

Scientific activity and notable results

Published articles

1. **H. Paşca**, A.V. Andreev, G.G. Adamian, N.V. Antonenko, and Y. Kim, *Energy dependence of mass, charge, isotopic, and energy distributions in neutron-induced fission of* ^{235}U *and* ^{239}Pu , Phys. Rev. C **93**, 054602 (2016);

2. **H. Paşca**, A.V. Andreev, G.G. Adamian, and N.V. Antonenko, *Unexpected asymmetry of the charge distribution in the fission of* ^{222}Th, ^{224}Th *at high excitation energies*, Phys. Rev. C **94**, 064614 (2016)

3. **H. Paşca**, A.V. Andreev, G.G. Adamian, and N.V. Antonenko, *Possible origin of transition from symmetric to asymmetric fission*, Phys. Lett. B **760**, 800 (2016).

4. **H. Paşca**, A.V. Andreev, G.G. Adamian, and N.V. Antonenko, *Extraction of potential energy in charge asymmetry coordinate from experimental fission data*, Eur. Phys. J. A **52**, 369 (2016)

Proceedings

1. **H. Paşca**, *Energy dependence of fission observables* , EPJ Web of Conferences **107** 07003 (2016),
DOI: 10.1051/epjconf/201610707003

2. **H. Paşca**, A.V. Andreev, G.G. Adamian, and N.V. Antonenko, *Physical origin of the transition from symmetric to asymmetric fission fragment charge distribution*, Accepted - will be published in Acta Physica Polonica **B46**, March 2017, Presented at the Zakopane Conference on Nuclear Physics Extremes of the Nuclear Landscape, Zakopane, Poland, August 28 September 4, 2016

3. **H. Paşca**, A.V. Andreev, G.G. Adamian, and N.V. Antonenko, *Physical origins of the transition from a symmetric to an asymmetric fission fragment charge distribution*, Proceedings of the Carpathian SSP16 Accepted - will be published at AIP. Presented at Carpathian Summer School of Physics (26 June- 09 July 2016), Sinaia, Romania.

Articles under review

1. **H. Paşca**, Sh. Kalandarov, G.G. Adamian, and N.V. Antonenko, *Spins of complex fragments in binary reactions within dinuclear system model*, sent to Phys. Rev. C.

Articles under preparation

1. **H. Paşca**, Sh. Kalandarov, G.G. Adamian, and N.V. Antonenko, *Possible explanation of the spin distribution structure in heavy-ion collisions*.

2. **H. Paşca**, A.V. Andreev, G.G. Adamian, and N.V. Antonenko *Fragment charge distributions originating from the fission of super-heavy elements* .

Participation to international conferences

1. **H. Paşca**, A. V. Andreev, G. G. Adamian, N. V. Antonenko, *"Energy dependence of the shape of the fission fragment charge distribution"*, 40th ASRC International Workshop "Experimental and Theoretical Advances in Fission and Heavy Nuclei ", Japan Atomic Energy Agency (JAEA), Tokai, Japan (12-13 December 2016);

2. **H. Paşca**, A. V. Andreev, G. G. Adamian, N. V. Antonenko, *Physical origin of the transition from symmetric to asymmetric fission fragment charge distribution*, Zakopane Conference on Nuclear Physics Extremes of the Nuclear Landscape, Zakopane, Poland, (August 28 September 4 2016);

3. **H. Paşca**, *"Physical origins of the transition from symmetric to asymmetric fission fragment charge distribution"* (Oral presentation), Carpathian

Summer School of Physics (26 June- 09 July 2016), Sinaia, Romania;

4. **H. Paşca**, *"Physical origin of transition from symmetric to asymmetric fission"* (Oral presentation), BLTP-KLTP Joint Workshop on Physics of Strong Interaction (28 June - 03 July 2016), Dubna, Russian Federation;

5. **H. Paşca**, *"Energy dependence of mass, charge, isotopic distributions and TKE in neutron-induced fission of ^{235}U and ^{239}Pu"* (Oral presentation), 119th Session of the Scientific Council of the Programme Advisory Committee for Nuclear Physics of JINR (18-19 February 2016), Dubna, Russian Federation; *The invitation to give this oral presentation was conditioned by the winning of the 1st place in the Poster Competition for Young Scientists at Programme Advisory Committee for Nuclear Physics of JINR.*

6. **H. Paşca**, *"Energy dependence of mass, charge, isotopic distributions and TKE in neutron induced fission of ^{235}U and ^{239}Pu"* (Poster), Programme Advisory Committee for Nuclear Physics of the Joint Institute for Nuclear Research (29-10 January 2016) in Dubna, Russian Federation; (*The poster won 1st place in the Poster Competition for Young Scientists*)

7. **H. Paşca**, *"Spin distribution of binary decay products"* (Oral presentation), 9th International Physics Conference of the Balkan Physical Union-BPU9 (24-27 August 2015), Istanbul, Turkey;

8. **H. Paşca**, *"Energy dependence of fission observables"* (Oral presentation), Nuclear Structure and Related Topics - NSRT15 (14-18 July 2015), Dubna, Russian Federation;

9. **H. Paşca**, *"Angular momentum distribution of binary reaction products"* (Oral presentation), SKLTP-BLTP JINR Joint Workshop on Physics of Strongly Interacting Systems (14-19 July 2014), Dubna, Russian Federation.

Seminars

1. 17th of October, Bogolyubov Laboratory of Theoretical Physics, JINR, Russian Federation, title *"Cluster approach for describing nuclear fission"* (Link: The list of seminars in 2016 at BLTP).

Awards

1. 1^{st} place in the Poster Competition for Young Scientists at Programme Advisory Committee for Nuclear Physics of JINR in 2016.

2. Received the JINR AYSS 2017 Grant (Grant No. 17-302-08, Link: Competition for JINR Young Scientists and Specialists.).

3. 1st place of the 2016 JINR Prize with the project *"Cluster approach for describing nuclear fission"*, authors: **H. Paşca**, G. Adamian, A. Andreev, N. Antonenko, R. Jolos, A. Nasirov, T. Shneidman.(Link: Jury's Decision on JINR Prizes for 2016).